Molecular Cancer

RESEARCH

Open Access

Transient intracellular expression of PD-L1 and VEGFR2 bispecific nanobody in cancer cells inspires long-term T cell activation and infiltration to combat tumor and inhibit cancer metastasis

Lei Zhang[1,2*†], Yunfeng Lin[1,3†], Li Hu[1,3], Yanan Wang[1,3], Chaohua Hu[4], Xinyi Shangguan[1,3], Shuzhi Tang[1], Jincan Chen[1], Ping Hu[1], Zhe-Sheng Chen[5], Zun-Fu Ke[6*] and Zhuo Chen[1,2*]

Abstract

Background PD-L1, an immune checkpoint inhibitor, and VEGFR2, essential for cancer metastasis, play pivotal roles in tumorigenesis. However, their miniature bispecific intracellular nanobodies for combining check-point blockade and anti-metastasis anticancer therapy remain underexplored.

Methods The intrabodies were developed using gene cloning technology. Specificity of the intrabodies was testified using Western blot, co-immunoprecipitation (co-IP) analysis, antibody competitive binding assay, flow cytometry analysis, etc. Checkpoint blockade was demonstrated using antibody-antigen competitive binding assay. Cancer cell migration was determined using scratch assay. Combined anti-cancer therapeutic efficacy of FAP1V2 was determined in vivo of mice models. The PD-1^{hi} immune cells, TCR β^{hi} and CD25^{hi} T-cells were analyzed by flow cytometry, and cancer cell metastasis was performed using immune-fluorescence analysis on lung and liver tissues. Transcriptome analysis was performed to explore signaling pathways associated with the enhanced anticancer efficiency.

Results Bispecific intrabody FAP1V2 fused with antibody V_H regions, was successfully developed and verified with its ability to target and block human and mouse PD-L1 and VEGFR2, inhibiting cancer cell binding to PD-1 and reducing their migratory capacity. Compared to the other treatment, two-rounds of transient FAP1V2 expression in LLC cells in experimental mice models achieved remarkable tumor inhibition, which brought about complete immune inhibition on growth of secondary-round of LLC tumor in 1/6 of the tested mice, inspired long-term activation of TCR β^{hi} T cells and increased their infiltration to tumors, inhibited the emergence of PD-1^{hi} immune cells, indicating prevented T cell depletion. The elevated CD25 expression also supported the success in enhancing immune response

†Lei Zhang and Yunfeng Lin contribute as co-first authors.

*Correspondence:
Lei Zhang
zhangl@fjirsm.ac.cn
Zun-Fu Ke
kezunfu@126.com
Zhuo Chen
zchen@fjirsm.ac.cn
Full list of author information is available at the end of the article

reported by elevated T cell activity in spleen. Transcriptome analysis identified critical intracellular pathways regulated by the concurrent blockade of PD-L1 and VEGFR2.

Conclusion PD-L1 and VEGFR2- bispecific V_H intracellular nanobody was highly biocompatible and showed the potential for combined anti-cancer therapy through long-term immune activation mediated by PD-L1/PD-1 checkpoint blockade and anti-metastasis mediated by VEGFR2 blockade.

Keywords Combination cancer therapy, Bispecific V_H intrabody, PD-L1, VEGFR2, Immune activation, T cell activation and infiltration, Anti-metastasis

Background

The failure of cancer therapy is often attributed to two major hurdles: ineffective drug treatment and inadequate immune response. Cancer cells can frequently evade drug-mediated cytotoxicity by developing drug resistance mechanisms [1–3], while immune cells, particularly T cells, often fail to effectively eliminate tumor cells. This failure in immune elimination is partially due to T cell exhaustion, a state characterized by impaired function and reduced proliferation of T cells in the tumor microenvironment [4–6]. Furthermore, the number and antitumor immune responses of tumor-infiltrating cytotoxic immune cells, especially T cells, are often significantly reduced [7, 8], limiting their ability to effectively target and kill tumor cells. Therapeutic approaches that can effectively activate the immune system to combat cancer are a promising area of research. One promising strategy involves targeting immune checkpoints, which are molecules expressed on immune cells that act as brakes on immune responses [9]. By blocking these checkpoints using monoclonal antibodies, the immune system can be unleashed to attack tumor cells more effectively. This strategy has shown remarkable success in various cancers, particularly in melanoma, lung cancer, and bladder cancer [10–13]. Examples of checkpoint inhibitors include anti-CTLA-4 antibodies such as ipilimumab and tremelimumab, and anti-PD-1 antibodies such as nivolumab and durvalumab [14–17]. Potentially by increasing the number and activity of tumor-infiltrating T cells, vaccines combined with immune checkpoint inhibitors can further enhance the anti-tumor efficacy [18].

Although evidence suggests that therapy utilizing antibodies such as the anti-PD-1 antibody sintilimab or cadonilimab, a bispecific antibody targeting PD-1 and cytotoxic T-lymphocyte antigen-4 therapies, can promote T cell infiltration and activity in the tumor microenvironment (TME) [19], these therapies may lead to reductions in levels of neutrophils, platelets, red blood cells causing anemia, or leukocytes [20, 21], which might be caused by blockage of potentially vital functions of these targets residing on immune cells. Current clinical antibodies contain substantial heterologous regions, such as the crystallizable fragment (Fc), leading to adverse effects and rapid clearance from the circulation. At present, the role of nanobody-mediated T cell activation versus direct T cell recognition of tumor antigens remains unclear. For instance, the ability of single-chain nanobodies lacking both the light chain variable region (V_L) and Fc regions to support endogenous T cell receptor (TCR) binding to tumor antigens and induce T cell activation [1, 22], especially following transient expression on tumor cells, is unknown. Further research exploring these critical aspects will be crucial to optimize current therapies and develop novel strategies for effective and durable cancer treatment.

PD-1 is an inducible protein expressed on activated T and B cells, and can also be found on NK cells, monocytes, and myeloid dendritic cells upon antigen induction [23, 24]. Prior to activation, T cells exhibit minimal PD-1 expression, which gradually increases following antigenic stimulation [25]. PD-L1, the functional ligand of PD-1, may act as a molecular "barrier" to protect PD-$L1^+$ tumor cells from $CD8^+$ T cell-mediated cancer cell elimination [26, 27], which is conducive to the escape of cancer cells from immune system. The binding of PD-L1 to PD-1 on tumor-infiltrating lymphocytes (TILs) transmits immunosuppressive signals, inhibiting the activation and function of antigen-specific cytotoxic T cells. This interaction consequently impairs the immune response, allowing tumors to evade recognition [28–30]. Recent findings have demonstrated that the interaction between PD-1 and its ligands (PD-L1 and PD-L2) leads to the attenuation of T cell activation [31]. The engagement of PD-1 by its ligands induces T cell differentiation into exhausted T cells, which are characterized by impaired proliferation, cytokine production, and cytotoxicity [32, 33]. Vascular endothelial cell growth factors (VEGFs) and their homologous receptors (VEGFRs) are crucial in neovascularization (or angiogenesis). They are upregulated in tumor vasculature and are a key factors in malignant growth of tumors [34], promoting tumor genesis, development and cancer cell metastasis [35–38]. VEGFR2 has strong tyrosine kinase activity, through binding to VEGF, leading to phosphorylation and activation of several downstream signaling proteins, including protein kinase B

(AKT), ERK1/2, and MAPK [39–42]. Blocking VEGFR2 signaling has been reported to inhibit tumor cell migration and inhibit angiogenesis [42–45]. Hitherto, there are currently no reports on how the blockade of PD-L1 and VEGFR2 on tumors by dual-target intrabodies affects PD-1 high (PD-1^{hi}) immune cells and T cell activation. This study reports the development of a novel bispecific nanobody, composed solely of variable regions of heavy chain (V_H), targeting both PD-L1 and VEGFR2 for tumor suppression. Its potential to mediate T cell infiltration and activation, thus facilitating anti-cancer immunotherapy, was investigated. Transcriptome sequencing and quantitative analysis were employed to elucidate the factors and signaling pathways involved in inhibiting tumor metastasis and modulating the immune response.

Materials and methods

Cell lines, media, antibodies and reagents

The human cervical cancer cell line HeLa, which was applied as a model cell line, was purchased from the Shanghai Institute of Cell Biology (Chinese Academy of Sciences) and was cultured in 1640 medium (Gibco) supplemented with 10% (*v/v*) fetal bovine serum (FBS, Gibco, Invitrogen, USA), 100 μg/mL penicillin and 100 μg/mL streptomycin (Gibco, Invitrogen, USA) at 37 °C with 5% CO_2.

HeLa cells transfected with plasmid *pEGFP-C1*, named as HeLa-EGFP, were used as the negative control. HeLa cells transiently transfected with plasmid *pEGFP-C1-AP1V2* (encoding FAP1V2), *pEGFP-C1-AP1* (encoding FAP1), or *pEGFP-C1-AV2* (encoding FAV2), respectively, were named as HeLa-FAP1V2, HeLa-FAP1, or HeLa-FAV2.

Rabbit anti-PD-L1, rabbit anti-VEGFR2, rabbit anti-GFP polyclonal antibodies, Rhodamine B 5-isothiocyanate (RBITC)-conjugated goat anti-rabbit IgG and Horseradish peroxidase (HRP)-conjugated goat anti-rabbit IgG were purchased from Sangon Biotech (Shanghai, China). Mouse anti-EGFP/GFP monoclonal antibodies, HRP-conjugated goat anti-mouse IgG and normal mouse IgG were purchased from Beyotime (Shanghai, China). PE-Labeled Human PD-1/PDCD1 Protein was purchased from Acrobiosystems (Bejing, China). Other antibodies used in immuno-fluorescent analysis were purchased from Servare Biotech Inc. (Wuhan, China).

Plasmid constructs

The recombinant bispecific intrabody *FAP1V2* gene sequence containing anti-PD-L1 V_H (*FAP1*), *EGFP* and anti-VEGFR2 V_H (*FAV2*) gene sequences was achieved by nucleotide polymerization (Sangon Biotech Co., Ltd., Shanghai, China). It was cloned into the mammalian expression vector *pEGFP-C1*, where *EGFP* as a fluorescence indicator was fused between the *FAP1* and *FAV2* for tracking transient (24–96 h) transgene expression of the intrabody. V_H genes and *EGFP* were connected via a short gene sequence encoding a flexible linker peptide $(GGGGS)_3$. The N-terminal of *FAP1* was fused with an IL-2 signal peptide (GenBank: AAD48509.1) and the C-terminal of *FAV2* was fused with a GPI anchor sequence (hPLAP, exon10, GenBank: M19159.1). This recombinant plasmid containing anti-PD-L1 and anti-VEGFR2 V_H sequences was named as *pEGFP-C1-AP1V2*. As the comparison with *pEGFP-C1-AP1V2* containing two V_H sequences, plasmid *pEGFP-C1-AP1* harboring only *AP1* gene sequence and *pEGFP-C1-AV2* harboring only *AV2* gene sequence were designed and constructed. The V_H sequences of the anti-PD-L1 antibody (PDB: 5XJ4) and the anti-VEGFR2 antibody (GenBank: ACH41918.1), respectively, were retrieved from the publicly available National Center for Biotechnology Information (https://www.ncbi.nlm.nih.gov/) database. The gene (*FAP1V2*) sequence of the dual targeting fusion V_H peptides specific for PD-L1 and VEGFR2, the primer sequences and the amino acid sequences of all fusion intrabodies used in this study are provided in Supplementary Tables 1–3.

Protein modeling and molecular docking

Homology models of the three-dimensional (3D) structures of FAP1V2 were obtained by submitting the FAP1V2 amino acid sequence to the Tencent iDrug platform (https://drug.ai.tencent.com/cn). The highest quality model was selected for further analysis. PD-L1 model structure was selected from PDB database (5X8M). We selected an existing 3D model from the ModBase as VEGFR2-ECD (extracellular domain) model (https://modbase.compbio.ucsf.edu/ Number: P35968.2). Docking analyses were performed focusing on PD-L1 or VEGFR2 as ligand binding to FAP1V2 model using the HDOCK program (http://hdock.phys.hust.edu.cn/). We selected the top 10 through the docking energy scores and overall root mean square deviation (RMSD). Next, the most appropriate docking models were selected according to the minimum distance between FAP1V2 V_H region and PD-L1 or VEGFR2-ECD, respectively. PyMOL software (The PyMOL Molecular Graphics System, Version 1.7, Schrodinger, New York, NY, USA) and PDBePISA (https://www.ebi.ac.uk/pdbe/) were used to visualize the modeled complexes, and the FAP1V2 residues that presumptively formed contact interface with the targets were identified.

Transfection

The cells were transfected according to the manufacturer's instructions of LipoFiter™ 3 (HANBIO, Shanghai,

China). HeLa cells were seeded one day before transfection, and the plasmid/ LipoFiter™ 3 complexes were added to the cell culture without serum when confluence of cells reached 70% the next day. After the cells were co-cultured with plasmid/ LipoFiter™ 3 complexes for 6 h, the serum-free medium containing plasmid/ LipoFiter™ 3 complexes was removed, and fresh medium containing 10% FBS serum was added. In this study, the dosage ratio of plasmid to LipoFiter™ 3 was 1:1 (w/v). For each well of the six-well plate, the dosage of plasmid was 4 μg and the dosage of LipoFiter™ 3 was 4 μL. After transfection, the cells were cultured for 48 h for subsequent experiments.

Transient expression of the FAP1, FAV2 or FAP1V2 intrabody

By the 48th h after transfection with recombinant plasmid, HeLa cells were lysed and sampled for PCR analysis of the *FAP1*, *FAV2* or *FAP1V2* gene, to determine whether the transfection was successful. HeLa cells were seeded in confocal petri dishes, transfected with recombinant plasmid and cultivated for 48 h. Fluorescence of EGFP was observed under laser confocal microscope (OLYMPUS Fluo View TMFV1000, Japan). By the 48th h after transfection with recombinant plasmid, HeLa cells were collected and lysed for Western blot analysis of EGFP expression that reported the expression of single-target or the dual-target V_H intrabody, using rabbit anti-GFP polyclonal antibody as the primary antibody and HRP-conjugated goat anti-Rabbit IgG as the secondary antibody.

Analysis of the ability of cell surficial PD-L1 or VEGFR2 to bind commercial antibodies

HeLa cells were seeded into 6-well plate at a density of 2×10^5/ mL medium. The plasmids used in Group 1 were *pEGFP-C1* (control), *pEGFP-C1-AP1*, and *pEGFP-C1-AP1V2*, and the plasmids used in Group 2 were *pEGFP-C1* (control), *pEGFP-C1-AV2*, and *pEGFP-C1-AP1V2*. The non-transfected HeLa cells were used to evaluate the background. Cells were treated by trypsin and collected by the 48th h of cell culture after transfection, fixed with 4% paraformaldehyde and washed with PBS for 3 times. The cells were incubated with the primary antibodies at room temperature for 1–2 h. The primary antibody used in Group 1 and Group 2 were rabbit anti- PD-L1 and anti-VEGFR2, respectively. After being washed with PBS for 3 times, the cells in both groups were incubated with RBITC-conjugated goat anti-rabbit IgG (the secondary antibody) at room temperature for 1 h. After washing with PBS for 3 times, the fluorescence of PD-L1 and VEGFR2 on HeLa cell surface were detected by flow cytometry through PE-A determination channel.

Analysis of the ability of intracellular PD-L1 or VEGFR2 to bind commercial antibodies

HeLa cells were seeded into confocal petri dishes at a density of 2×10^5/ mL medium, and two same experimental groups as have been described in the above method for flow cytometry were transfected according to the manufacture's instruction. The cells were then fixed with 4% paraformaldehyde, carefully washed with PBS three times, and blocked with 5% BSA (in PBS). Then the cells were incubated with primary antibody (1:1000 in PBS containing 5% BSA and 0.1% Triton X-100), washed 3 times with PBS, followed by incubation with RBITC-conjugated secondary antibody. The cells were washed 3 times with PBS, stained with DAPI (10 μg/mL), added with 1 mL PBS observed under a confocal laser scanning microscope (CLSM) and photographed for analysis of the fluorescence distribution and intensity.

Co-immunoprecipitation

HeLa cells were seeded into the 6-well plate at a density of 2×10^5/mL medium for transfection. By 48th h after transfection, pre-cooled cell lysate buffer (Beyotime, China) was added. Cells were scraped with a cell scraper and the cell lysate suspensions were collected. Then the mouse originated normal IgG (to exclude non-specific binding) and Protein A + G agarose (Beyotime, China) were added to the cell lysate suspensions. After 1 h incubation at 4 °C on the mixer, the supernatant was centrifuged at 2,500 × g for 5 min and collected for immunoprecipitation. Protein A + G agarose at the bottom of the tube was precipitated and set as the control. The incubated cell suspension was transferred into a new 1.5 mL EP tube, and mouse anti-EGFP IgG was added into the tube and incubated on the mixer at 4 °C overnight. Protein A + G agarose was then added into the EP tube and incubated on the mixer at 4 °C for 4 h, centrifuged at 2,500 × g for 5 min, and the supernatant was removed. The Protein A + G agarose precipitate at the bottom of the tube was washed with cell lysate buffer for 5 times, then SDS-PAGE loading buffer was added to the precipitates and the mixture was boiled for 5 min, and then the samples were separated on by SDS-PAGE gel electrophoresis. The proteins within the gel were then transferred to a 0.22 μm PVDF membrane using Trans-Blot Turbo Transfer System (BioRad) and the membrane was pre-incubated with 5% fat-free milk (in TBST) for 2 h at RT. The membranes were then incubated with primary antibody at 4 °C overnight followed by thorough wash with TBST and incubation with HRP-conjugated secondary antibodies at room temperature for 2 h. Protein bands were visualized by AI600 RGB imaging system

(Amersham Imager 600, GE, USA) after incubation with BeyoECL Star (Beyotime, China).

Analysis of the ability of cell surficial PD-L1 to bind PE-labeled human PD-1 protein

HeLa cells were seeded into 6-well plate at a density of 2×10^5/mL medium. The plasmids for transfection were *pEGFP-C1* (the control), *pEGFP-C1-AP1* and *pEGFP-C1-AP1V2*, and the non-transfected HeLa cells were used to evaluate the background. Cells were collected by the 48th h of culture after transfection, fixed with 4% paraformaldehyde and washed with PBS for 3 times. The cells were incubated with the PE-Labeled Human PD-1 Protein on the mixer at 4 °C overnight. After washing with PBS for 3 times. The fluorescence intensity showing abundance of PD-L1 on HeLa cell surface was determined by flow cytometry through PE-A determination channel.

Cell viability assays

For cell viability assay, cells (3×10^3 cells per well) were seeded into 96-well plates and transfected according to the method described above. The plasmids for transfection were *pEGFP-C1*, *pEGFP-C1-AP1, pEGFP-C1-AV2* and *pEGFP-C1-AP1V2*. After 44 h, the medium was replaced with new fresh medium containing 3-(4, 5-dimethylthiazol-2-yl)−2, 5-diphenyltetrazolium bromide (MTT) solution (Beyotime, China) and cultured for an additional 4 h at 37 °C. Subsequently, the medium was removed, and DMSO was added into the medium to dissolve the purple crystals at 37 °C. Finally, the absorbance was determined in Synergy™ H4 Multi-Mode Microplate Reader (BioTek, USA) at a wavelength of 490 nm.

Detection of competitive binding of FAP1V2 to LLC mouse cells (expressing PD-L1 and VEGFR2) in the presence of commercial antibodies

Two hundred and ninety-three T cells were seeded at a density of 3×10^5 cells per well in a 6-well plate and allowed to adhere overnight, and transfected with plasmids *pEGFP-FAP1*, *pEGFP-FAV2*, and *pEGFP-FAP1V2* without endotoxin using lipid transfection reagent (HANBIO, Shanghai, China). The cells were lysed using RIPA lysis buffer containing Protease Inhibitor Cocktail (Selleck) and Phosphatase Inhibitor Cocktail II (MCE), centrifuged at 12,000×g (4 °C) for 15 min, and the supernatant was then collected.

The LLC cells in logarithmic growth phase were fixed with 4% paraformaldehyde at room temperature for 30 min, centrifuged at 2,000×g for 2 min, and the supernatant was discarded. The cells were then blocked with 5% BSA (dissolved in PBS) at room temperature for 1 h, centrifuged at 2,000×g for 2 min, and the supernatant was discarded. The cells were incubated with 293T cell lysate containing FAP1, FAV2 or FAP1V2 at room temperature for 30 min, followed by incubation with commercial rabbit-derived Anti-mouse PD-L1-APC or Anti-mouse VEGFR2-APC (Elabscience, Wuhan, China) at room temperature for 30 min. After centrifugation at 2,000×g for 4 min and removal of the supernatant, 200 μL of fresh medium was added for flow cytometry analysis (using APC detection channel).

In vivo study of the immune resistance to LLC tumors

Since the intrabodies also showed the ability to target and bind mice originated PD-L1 and VEGFR2 which have high similarity to those of human, in vivo experiments were carried out in C57BL/6 as tumor-bearing model mice according to the following methods. In detail, C57BL/6 mice were randomly divided into 4 groups with 6 mice in each group. LLC cells were transparently transfected with plasmids containing *FAP1*, *FAV2* and *FAP1V2* genes and empty plasmids according to the manufacturer's instructions., using lipofiter (HANBIO, Shanghai, China) as transfection reagent. The transfected LLC cells (1×10^7) were subcutaneously injected into the right armpit of C57BL/6 mice in each group to construct tumor bearing model. Four days later, the transfected LLC cells (1×10^7) were re-inoculated into the left armpit of each group of mice. The total transgene expression sustained for approximately 7–8 days, so that immune response could be promoted. Throughout the experiment, each mouse in different groups was labeled and tracked separately. Tumor size and animal weight were recorded once a day, and tumor volume was calculated with the following formula: $V\ tumor = Length \times Width \times Height \times \pi/6$.

After total 4 weeks, the mice were sacrificed by dislocation, and the tumors were stripped and photographed. In addition, important organs (heart, liver, spleen, lung, kidney and stomach) were cut into small pieces, fixed with 4% formalin and embedded in paraffin. Then the paraffin embedded tissues were sectioned and H&E staining was performed, and the histopathological analysis of important organs was carried out. Immunofluorescence microscopy was used to analyze distribution and levels of $PD\text{-}1^{hi}$ and TCR β^{hi} immune cells in tumors and spleens. The variance of activated T cells ($CD25^{hi}$) numbers in spleen was determined using Anti-Mouse CD25 APC (Clone: PC61.5) combined with flow cytometry analysis after the spleen had undergone grinding and treatment with collagenase, hyaluronidase and DNase I (Tansoole Platform, Fuzhou, China).

Determination of cell migration and metastasis

HeLa and LLC cancer cells expressing both high levels of PD-L1 and VEGFR-2 were seeded into the 6-well plate and transfected as described. The plasmids for

transfection were *pEGFP-C1* (the control), *pEGFP-C1-AP1*, *pEGFP-C1-AV2* and *pEGFP-C1-AP1V2*, and the non-transfected cells were used to evaluate the background. By the 24th hour after cell transfection, a 200 μL pipette tips (Titan, China) was used to scratch the vertical orifice plate, and the scratch time was recorded as 0 h. Subsequently, PBS was carefully added to wash the cells for 2–3 times. The cell medium was then replaced with low serum (2%) medium and photographed. The cell culture was sustained at 37 °C with 5% CO_2. The cell status was observed and photographed every 12 h until the gaps of non-transfected cells were healed. Image J was used to process the Image, and 7 horizontal lines were drawn randomly to calculate the migrated distance. Metastatic LLC cells were determined in the lungs and livers from each mice model group using VEGFR2 (overexpressed in LLC cells) as a biomarker. Migration distance was calculated according to formula $D=(A_{initial}-A_{measured})/W$, where D represents distance of migration, $A_{initial}$ represents initial unhealed area (before healing); $A_{measured}$ represents unhealed area at the time of measurement; W represents width of the photograph at the same magnification. This experiment was conducted at least three times.

Transcriptome sequencing and differential expression analysis

Total RNA was extracted from HeLa cells of each group using the TRzol® Reagent (Invitrogen, USA) according to the manufacturer's protocols. Bioanalyser 2100 (Agilent Technologies, PaloAlto, CA, USA) was used to evaluate the quality of RNA and ND-2000 (NanoDrop Technologies, Inc. Wilmington, DE, USA) was used to quantify RNA. The RNA-seq transcriptome library was constructed using the RNA samples (5 μg). The messenger RNA (mRNA) was fragmentated using fragmentation buffer and isolated by polyA selection with oligo (dT) beads. According to Illumina's library construction protocol, cDNA originated double-stranded DNA (dscDNA) fragments were synthesized, and the target cDNA fragments of 200–300 bp were selected for PCR amplification (15 PCR cycles) using Phusion DNA polymerase (NEB) after end-repair, phosphorylation and 'A'-base addition. Illumina HiSeq 4000 (2×150 bp read Length) was used for sequencing (Majorbio Biotech Co., Ltd, Shanghai, China). After map reading [46], differential expression genes (DEG) between two different samples were identified according to the fragments per kilobase of exon per million mapped reads (FRKM) method [47].

Data acquisition and statistical analysis

Immunofluorescence analysis was acquired using confocal fluorescence microscopy at identical settings for each of the experimental conditions. All data are presented as the Mean ± SEM. Comparisons between two groups were performed by unpaired, two-tailed t-test. For more than two groups, one-way ANOVA followed by two-way ANOVA analysis was performed using Prism 6.0 software (GraphPad). Results with $p<0.05$ were considered significant. P values are summarized as: $^{*}P\leq0.05$, $^{**}P\leq0.01$, and $^{***}P\leq0.001$, unless stated otherwise.

Results and discussion

Structural base for V_H based FAP1V2 nanobody to bind PD-L1 and VEGFR2

By simultaneously blocking PD-L1 and inhibiting VEGFR2 signaling, this approach aims to activate T-cell function and suppress cancer cell metastasis. To address limitations associated with conventional antibodies, such as inefficient intracellular delivery, the nanobody design omits the Fc fragment and V_L light chain, which traditionally stabilizes the V_H heavy chain. This modification minimizes immunogenicity and size [48], enabling intracellular expression of an engineered chimeric gene. While most single-chain antibodies include both V_L and V_H fragments, we hypothesize that single V_H chains, due to their smaller size, might exhibit sufficient flexibility for antigen binding. Furthermore, the specificity of these intrabodies to tumor-associated antigens (TAAs) holds potential for investigating signaling pathways regulated by intracellular TAAs.

The bispecific intrabody FAP1V2 targeting PD-L1 and VEGFR2 comprised IL-2 signal, anti-PD-L1 V_H region, $(GGGGS)_3$ linker, EGFP section, $(GGGGS)_3$ linker, anti-VEGFR2 V_H region, and GPI anchor (Fig. 1A). The IL-2 signal was designed at the N-terminus for guiding FAP1V2 to the outer cell space. The GPI anchor peptide was linked to the C-terminus for anchoring FAP1V2 on cell surface, allowing them to interact with the surface PD-L1 and VEGFR2 antigens. EGFP was designed as reporter for the transient expression of AP1V2 and as an indicator for tracking the cellular location of FAP1V2; it also functioned as spacer between AP1 and AV2. To investigate the potential of FAP1V2 to bind its targets, PD-L1 and VEGFR2, the three-dimensional (3D) models of FAP1V2 were computerized, and the binding sites were calculated by docking analysis. The FAP1V2 model showed a "clip" form composed of two V_H regions, EGFP section (Fig. 1B). The interaction between FAP1V2 and PD-L1 potentially included five hydrogen bonds (FAP1V2 Arg^{19} with PD-L1 Val^{51}, FAP1V2 Arg^{19} with PD-L1 Glu^{54}, FAP1V2 Ser^{170} with PD-L1 Tyr^{106}, FAP1V2 Ser^{17} with PD-L1 Tyr^{39}, and FAP1V2 Gln^{82} with PD-L1 Gln^{49}), two salt bridges (Between FAP1V2 Arg^{19} and PD-L1 Glu^{54}, FAP1V2 Arg^{19} and PD-L1 Asp^{56}), whereas no disulfide bonds or covalent bonds were found (Fig. 1C, Supplementary Table 4). The interface between

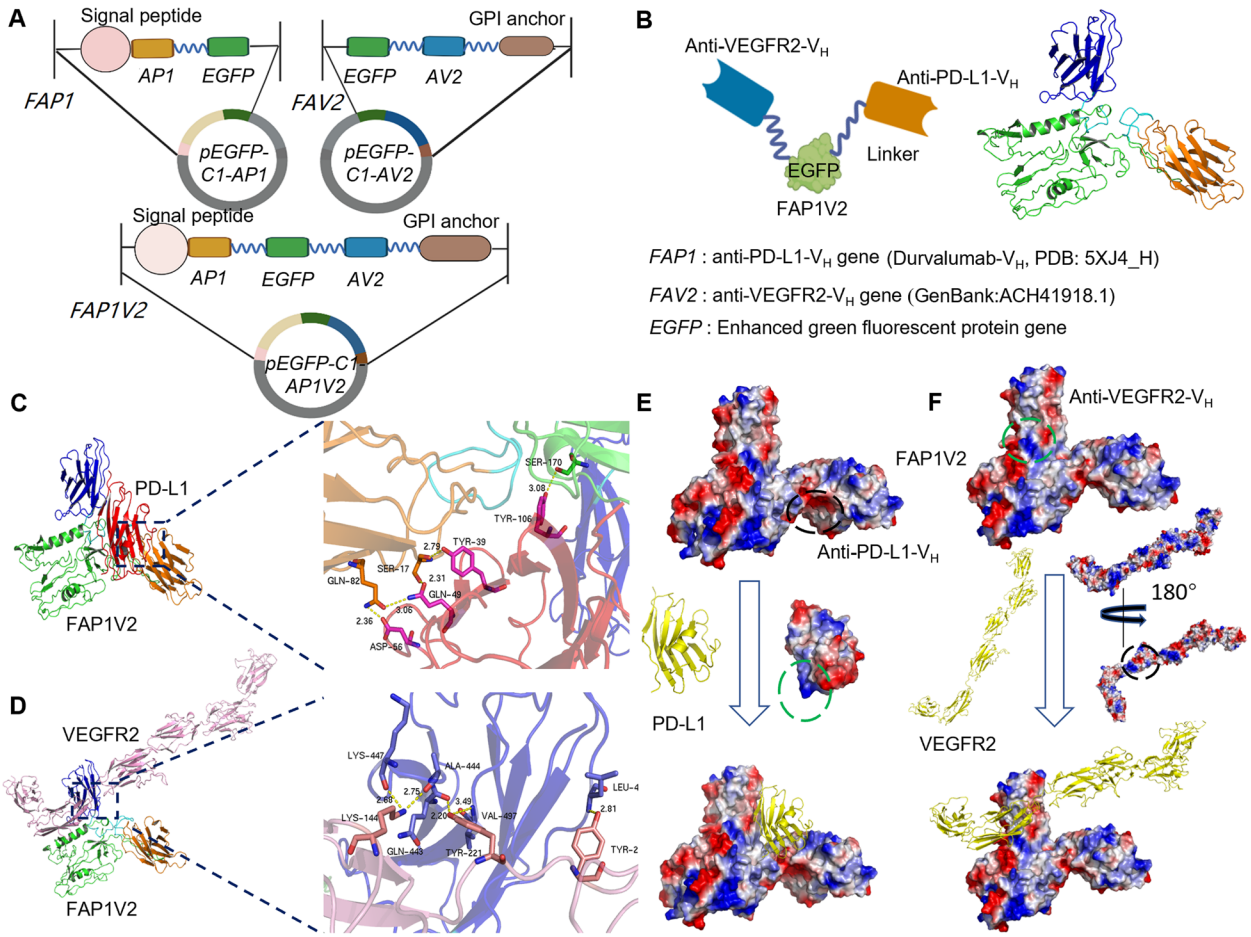

Fig. 1 Design of the intrabodies and molecular docking of FAP1V2/PD-L1 or FAP1V2/VEGFR2 complex. **A** The recombinant bispecific intracellular antibody gene (*FAP1V2*) sequence contains IL-2 signal, anti-PD-L1 V_H gene (*AP1*) and anti-VEGFR2 V_H gene (*AV2*), EGFP reporter, and GPI anchor. *pEGFP-C1-AP1* harbors *FAP1* and *pEGFP-C1-AV2* harbors *FAV2*. **B** The 3D model of FAP1V2. The orange region depicts anti-PD-L1 V_H (AP1), and the dark blue region depicts anti-VEGFR2 V_H (AV2). The green region depicts EGFP, which was fused with anti-PD-L1 V_H and anti-VEGFR2 V_H via $(GGGGS)_3$ linkers (shown in light blue), respectively. **C** and (**D**) Molecular docking and binding site prediction for FAP1V2 in complex with PD-L1 (red) and VEGFR2-ECD (pink), respectively. **E** The contact potential between FAP1V2 and PD-L1. **F** The contact potential between FAP1V2 and VEGFR2. The positively charged region was pointed out by black circle and the negatively charged region was pointed out by green circle. Blue and red colors in the electrostatic surface diagrams correspond to positive and negative electrostatic potentials at neutral pH, respectively

FAP1V2 and VEGFR2-ECD (extracellular domain) (Fig. 1D, Supplementary Table 5) was maintained by four hydrogen bonds (FAP1V2 Val^{497} with PD-L1 Tyr^{221}, FAP1V2 Phe^{513} with PD-L1 Asp^{131}, FAP1V2 Ala^{444} with PD-L1 Lys^{144}, and FAP1V2 Gln^{443} with PD-L1 Tyr^{221}), whereas no salt bridges or disulfide bonds or covalent bonds were revealed. Analysis of surface electrostatic potential energy (Fig. 1E) shows the contact potential between FAP1V2 and PD-L1. The charge of the positively charged region of FAP1V2 (Arg^{19}, Lys^{168} and Lys^{183}) provided electricity base for FAP1V2 to bind the negatively charged region of PD-L1 (Glu^{41}, Glu^{43}, Asp^{44}, Glu^{54} and Asp^{56}). Figure 1F shows the contact potential between FAP1V2 and VEGFR2. The negatively charged region of FAP1V2 (Glu^{314}, Asp^{315}, Asp^{376}, Glu^{377} and Asp^{514}) has strong electrostatic interaction with the positively charged VEGFR2 region (His^{133}, Lys^{144}, Lys^{168}, Arg^{222}, Lys^{316} and Lys^{317}).

HeLa cells expressed intrabodies by cell transfection

Two cell lines, HeLa human cervical cancer cells and LLC mouse Lewis lung carcinoma cells, were selected for this study due to their expression of PD-L1 and VEGFR-2, which are actively studied in the development of targeting therapeutic agents [49–53]. HeLa cells were used as a model cell line for in vitro experiments, while LLC cells were used as a model cell line for immune-related experiments in tumor-bearing mice. The predicted molecular

weights of FAP1 and FAV2 were about 42 kDa, and that of FAP1V2 was approximately 57 kDa. PCR analysis of the cell lysates indicated successful transfection of the intrabody genes *FAP1V2*, *FAP1*, and *FAV2* in HeLa cells (Supplementary Fig. 1). Confocal laser scanning microscopy (CLSM) analysis showed the cellular expression and distribution of the recombinant intrabodies FAP1, FAV2, and FAP1V2 (Fig. 2A; magnified in Supplementary Fig. 1). Western blot analysis results indicated successful expression of these fusion V_H intrabodies in HeLa cells (Fig. 2A, Supplementary Fig. 1). According to these results, we conclude that the recombinant plasmid was transfected into HeLa cells and induced successful expression of FAP1, FAV2, and FAP1V2.

Specificity of FAP1V2 against PD-L1 and VEGFR2

To demonstrate the specificity of FAP1V2 against PD-L1 and VEGFR2, co-immunoprecipitation (co-IP) analysis was performed. In-put results showed that EGFP (or FAP1V2 containing EGFP), PD-L1 and VEGFR2 could be detected in total lysates of HeLa-EGFP or HeLa-FAP1V2 cells, respectively (Fig. 2B). Co-IP results showed that only EGFP but not PD-L1 or VEGFR2 was captured from the lysates of HeLa-EGFP cells due to lack of FAP1V2 expression. However, PD-L1 and VEGFR2 were captured from the lysates of HeLa-FAP1V2 cells expressing FAP1V2 (Fig. 2B). These results demonstrated that FAP1V2 was expressed by HeLa-FAP1V2 cells and can specifically bind to PD-L1 and VEGFR2.

FAP1V2 blocked the target-binding ability of PD-L1 and VEGFR2

The V_H sequences of the anti-PD-L1 antibody (PDB: 5XJ4) and that of the anti-VEGFR2 antibody (GenBank: ACH41918.1) have been reported with demonstrated high specificity for their respective antigens. Nonetheless, as we have integrated EGFP into the V_H regions, and considering that EGFP does not bind to majority of known proteins, it is important to verify whether the newly formed fusion intrabodies maintain high-affinity binding to their targets after the incorporation of EGFP. In additional, if the new intracellular antibody exhibits comparable or improved affinity for the antigens relative to commercial antibodies, it may offer significant potential for efficient antigen blockade, thereby establishing a foundation for the efficacy of subsequent combined therapies targeting PD-L1 and VEGFR2 simultaneously. We then used the commercial RBITC-labelled anti-PD-L1 or RBITC-labelled anti-VEGFR2 antibody, respectively, to compete the PD-L1 or VEGFR2 from binding with FAP1V2. Flow cytometry analysis showed that, as compared with the control group transfected with vector plasmid *pEGFP-C1*, the ability of PD-L1 to bind commercial antibodies in the cells expressing FAP1 or FAP1V2 was significantly inhibited (Fig. 2C and D). Similarly, the ability of VEGFR2 to bind commercial antibodies also remarkably declined in the cells expressing FAV2 or FAP1V2 compared with the control group (Fig. 2E and F). Table 1 shows quantitative data for cell surficial PD-L1 and VEGFR2 to bind fluorescent antibodies after the cells were transfected with the above plasmids. CLSM analysis further confirmed that much fewer commercial antibodies could bind intrinsic PD-L1 or VEGFR2, which was caused by the binding between FAP1V2 and PD-L1 or the binding between FAP1V2 and VEGFR2, which led to the occupation of the smaller intrabody (FAP1V2) at the epitopes of PD-L1 or VEGFR2 that could originally bind the commercial antibodies (Fig. 2G-J). It should be noted that when we analyzed the blockage of the cell surficial PD-L1 or VEGFR2 by FAP1V2, the cells were not treated with Triton, which was frequently applied to increase permeation of the cell membranes. In CLSM analysis, the cells were treated with Triton, and the ability of whole cellular PD-L1 or VEGFR2 to bind FAP1V2 was demonstrated. Taken together, these data demonstrate that FAP1V2 can directly bind and block the cell surficial and intracellular PD-L1 and VEGFR2. Which led to inhibition of their ability to bind commercial antibodies. The results of this experiment indicate that with incorporation of EGFP, the intrabodies keep high affinity and strong blockade effect of toward their antigens, while also excluding the possibility of EGFP to reduce their binding ability to the antigens and potential background fluorescence of EGPF.

FAP1V2 inhibited the PD-L1/PD-1 checkpoint and enhanced T-cell-mediated immune inhibition in vivo

The ability of cell surficial PD-L1 to bind commercial fluorescent human PD-1 [labeled by phycoerythrin (PE)] was determined in HeLa cells by flow cytometry (Fig. 3). Compared with the control HeLa cell group transfected with *pEGFP-C1*, the ability of PD-L1 on HeLa-FAP1 or HeLa-FAP1V2 cell surface to bind PE-labeled commercial PD-1 remarkably decreased. This inhibition occurred on HeLa-FAP1 cell surface was a bit more obvious (Fig. 3B). This phenomenon suggests that the V_H-originated fusion intrabodies FAP1V2 and FAP1 expressed by HeLa cells can block PD-L1 and inhibit the binding of PD-L1 and PD-1 effectively. This could be caused by the inhibited ability of PD-L1 to bind PD-1 during binding to the intrabodies, accompanied by the inhibited transmembrane transportation of PD-L1 to the cell surface caused by structural blockage by the intrabodies.

Cell flow cytometry and antibody competition assays demonstrated that intracellular antibodies FAP1 and FAP1V2 could selectively block mouse PD-L1 expressed

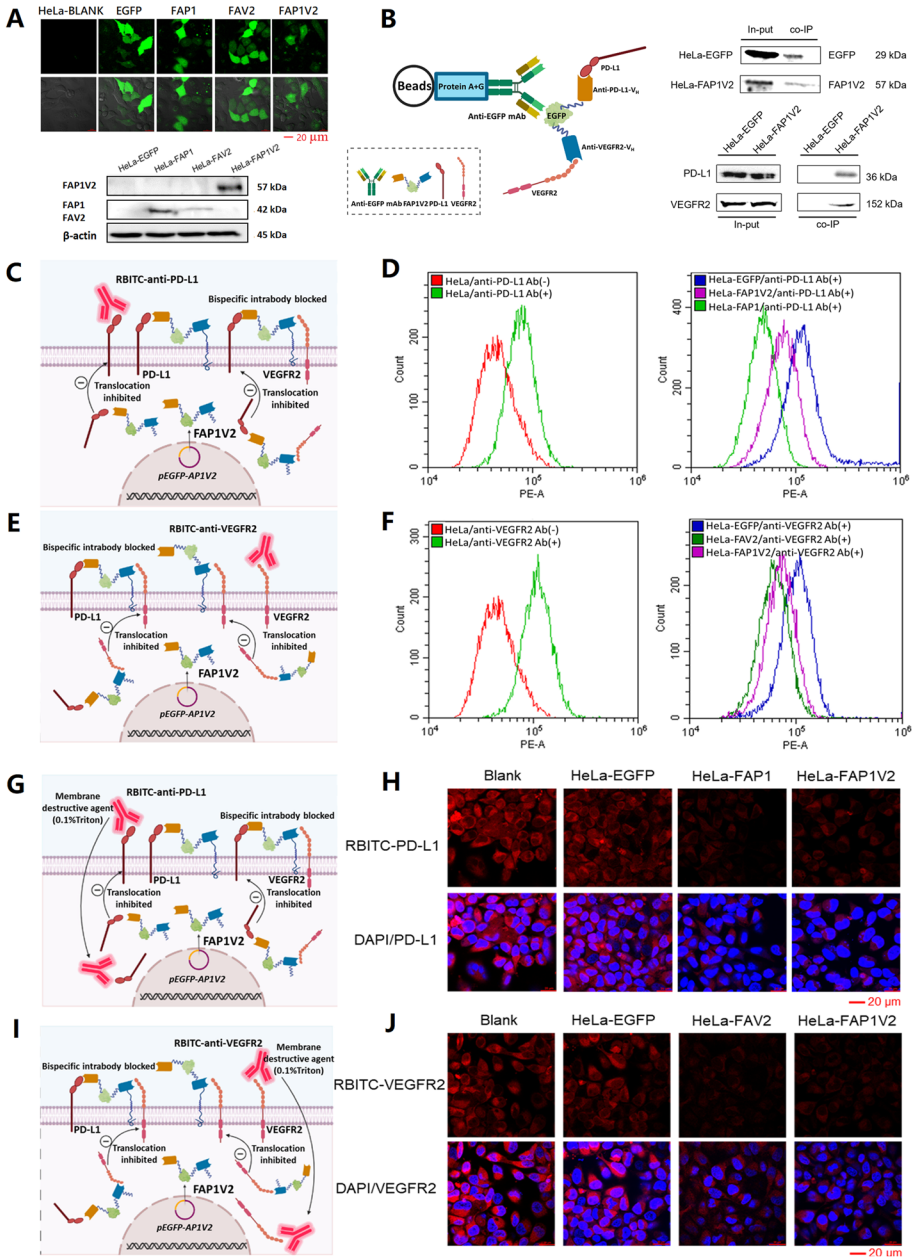

Fig. 2 Specific binding of FAP1V2 to PD-L1 and VEGFR2 led to efficient inhibition of tumor progress. **A** CLSM and Western blot analysis of transient expression of the intrabody genes in HeLa. **B** Co-immunoprecipitation assay of the dual-specificity of FAP1V2 against PD-L1 and VEGFR2. In the left panel, the schematic diagram was shown. In the right panel, PD-L1 and VEGFR2 in the input and co-immunoprecipitated components were analyzed by Western blot. The MW of PD-L1 was 36 kDa, and the MW of VEGFR2 was 152 kDa. The MW of EGFP was 29 kDa. **C** Schematic diagram and (**D**) flow cytometry assay showed that the blockage of cell surficial PD-L1 by FAP1V2 caused the reduced activity of PD-L1 to bind commercial antibodies. The cells were not treated with Triton. **E** Schematic diagram and (**F**) flow cytometry assay showed that the blockage of cell surficial VEGFR2 by FAP1V2 caused reduced activity of VEGFR2 to bind commercial antibodies. The cells were not treated with Triton. **G** Schematic diagram and (**H**) CLSM analysis showed that the blockage of intracellular PD-L1 by FAP1V2 caused reduced activity of PD-L1 to bind commercial antibodies. The cells were treated with 0.1% Triton. **I** Schematic diagram and (**J**) CLSM analysis showed that the blockage of intracellular VEGFR2 by FAP1V2 caused reduced activity of VEGFR2 to bind commercial antibodies. The cells were treated with 0.1% Triton. For all the above experiment, the red fluorescence showed RBITC-labeled commercial antibody specific for PD-L1 or VEGFR2, and the blue fluorescence showed cell nuclei stained by DAPI. The ability of PD-L1 and VEGFR2 to bind the commercial antibodies was determined after transient transfection of HeLa cells with plasmids *pEGFP-C1*, *pEGFP-C1-AP1*, *pEGFP-C1-AV2* or *pEGFP-C1-AP1V2*, respectively

Table 1 Mean fluorescence intensity showing the binding between cell surficial PD-L1 or VEGFR2 to commercial antibodies[a]

Primary Antibodies	Mean fluorescence intensity of RBITC			
	HeLa-EGFP	HeLa-FAP1	HeLa-FAV2	HeLa-FAP1V2
Anti-PD-L1 Ab (+)	391,871.0	51,394.4	-	77,166.0
Anti-VEGFR2 Ab (+)	111,562.1	-	72,572.3	81,118.6

[a] Flow cytometry was used to determine the fluorescence after HeLa cells were transfected with *pEGFP-C1*, *pEGFP-C1-AP1*, *pEGFP-C1-AV2* or *pEGFP-C1-AP1V2*, respectively. RBITC-conjugated secondary antibody was then used. The fluorescence intensity showing abundance of commercial antibodies on cell surface was determined by flow cytometry through PE-A determination channel

by mouse Lewis Lung Carcinoma (LLC) cells (Fig. 3C, D), and these intracellular antibodies separately expressed in 293 T cells could remarkably compete the blockade of commercial anti-mouse PD-L1 antibodies [conjugated with allophycocyanin (APC)] on PD-L1 in LLC cells (Fig. 3C, D). Similarly, competition blockade on mouse VEGFR2 against commercial anti-mouse (VEGFR2) antibodies was observed with FAV2 and FAP1V2 (Fig. 3E, F).

In vitro experiment demonstrated that, when HeLa or non-tumor cells were tested under non-immune conditions, the intracellular expression of these intrabodies showed decent biocompatibility (Supplementary Fig. 2). In vivo, immune enhanced inhibition on tumors was subsequently performed based on the mouse model. Following two transient intrabody expressions (each sustained for 24–96 h) in LLC cells, the anti-PD-L1-anti-VEGFR2 chimeric intrabody FAP1V2 demonstrated superior immune suppression of LLC cell tumorigenesis and growth in C57BL/6 mice. FAP1 exhibited a less pronounced inhibitory effect. FAV2 expression brought about medium effects, *i.e.*, the tumor growth rate was inhibited to approximately 50% compared with the control, which did not express the intrabodies. Secondary tumors, which transiently expressed the intrabodies and were established four days after primary tumor inoculation, exhibited significantly enhanced immune inhibition compared to primary tumors, and intracellular expression of FAP1V2 in LLC cells achieved best performance to inhibit tumor growth. Among the 6 tested mice inoculated with LLC cells which expressed FAP1V2 transiently, one mouse was not detected with LLC tumor growth completely. Mice that did not express intrabodies were in the control group (Fig. 3G-I).

TCR β is crucial for the activation of T cells and the specificity of the immune response [54, 55].

(See figure on next page.)

Fig. 3 Efficacy of FAP1V2 transient expression in mediating PD-1 checkpoint blockade immune inhibition of LLC progress in mice models. **A** Schematic diagram and (**B**) flow cytometry assay showed that the blockage of cell surficial PD-L1 by FAP1V2 or FAP1 caused reduced activity of PD-L1 to bind commercial PE-labeled human PD-1. The cells were transfected with *pEGFP-C1*, *pEGFP-C1-AP1* or *pEGFP-C1-AP1V2*, respectively. The cells were not treated with 0.1% Triton before cell cytometry analysis. **C** to (**F**) Cell flow cytometry and antibody competition assays demonstrated that intracellular antibodies FAP1 and FAP1V2, or FAV2 and FAP1V2 could selectively bind to PD-L1 or VEGFR2 expressed by LLC cells. Initially, 293 T cells were separately transfected with *pEGFP-C1-AP1*, *pEGFP-AV2* or *pEGFP-C1-AP1V2*. Following co-incubation of their lysates with LLC cells (fixed with paraformaldehyde), competitive binding assays were performed using commercial anti-mouse PD-L1 and VEGFR2 antibodies (conjugated with APC) against the corresponding antigens. Panel **(C)** shows LLC cells in four conditions, from left to right: Control: No co-incubation with 293 T lysates or commercial antibody. Anti-PD-L1 antibody: Co-incubated with commercial anti-mouse PD-L1 antibody. Single-target intrabody (FAP1) plus anti-PD-L1 antibody: Co-incubated with 293 T lysate expressing single-target intrabody FAP1, followed by addition of commercial anti-mouse PD-L1 antibody. Double-target intrabody (FAP1V2) plus anti-PD-L1 antibody: Co-incubated with 293 T lysate expressing double-target intrabody FAP1V2, followed by addition of commercial anti-mouse PD-L1 antibody. **D** Column graph illustrates the average fluorescence values of results shown in (**C**). Panel (**E**) shows LLC cells in four conditions, from left to right: Control: No co-incubation with 293 T lysates or commercial antibody. Anti-VEGFR2 antibody: Co-incubated with commercial anti-mouse VEGFR2 antibody. Single-target intrabody (FAV2) plus anti-PD-L1 antibody: Co-incubated with 293 T lysate expressing single-target intrabody FAV2, followed by addition of commercial anti-mouse VEGFR2 antibody. Double-target intrabody (FAP1V2) plus anti-VEGFR2 antibody: Co-incubated with 293 T lysate expressing double-target intrabody FAP1V2, followed by addition of commercial anti-mouse VEGFR2 antibody. **F** Column graph presents the average fluorescence values of results shown in (**E**). This experiment was independently repeated three times. Based on three mean fluorescence values (MFV) of the cell populations from each sample, as reported by flow cytometer (Channel APC-A), the data for the mean fluorescence values detected at Channel APC-A are presented as Mean $_{MFV}$ ± SEM. *, **, *** represent significant differences compared to the control group at the levels of $P < 0.05$, $P < 0.01$, $P < 0.001$, respectively. #, ##, ### indicate significant differences between treatment groups at the levels of $P < 0.05$, $P < 0.01$, $P < 0.001$, respectively. **G** to (**I**) The effect of anti-PD-L1-anti-VEGFR2 chimeric intrabody FAP1V2 on enhancing immune activity of suppressing tumorigenesis and growth of LLC cells in C57BL/6 mice. **G** Timeline for studying transient FAP1V2 expression mediated anticancer therapy via immune activation and antimetastatic effects. **H** Tumor size varied in the mice injected with LLC cancer cells which transiently expressed FAP1, FAV2 or FAP1V2 intrabody, respectively. The group of mice inoculated with LLC cells transiently transfected with blank plasmid (*pEGFP-C1*) were set as a control. The LLC cells were respectively subcutaneously injected to the right armpits first and then to the left armpits 4 days later, which can maintain the transient expression of the intrabodies for total 6–8 days in the beginning. The data on tumor sizes for each group, which included tumors located in the same side of armpits from 6 mice, are presented as the Mean $_{Tumor\ size}$ ± SEM. **(I)** Images of the tumors separated from the right and left armpits of the mice which were sacrificed at Day 28

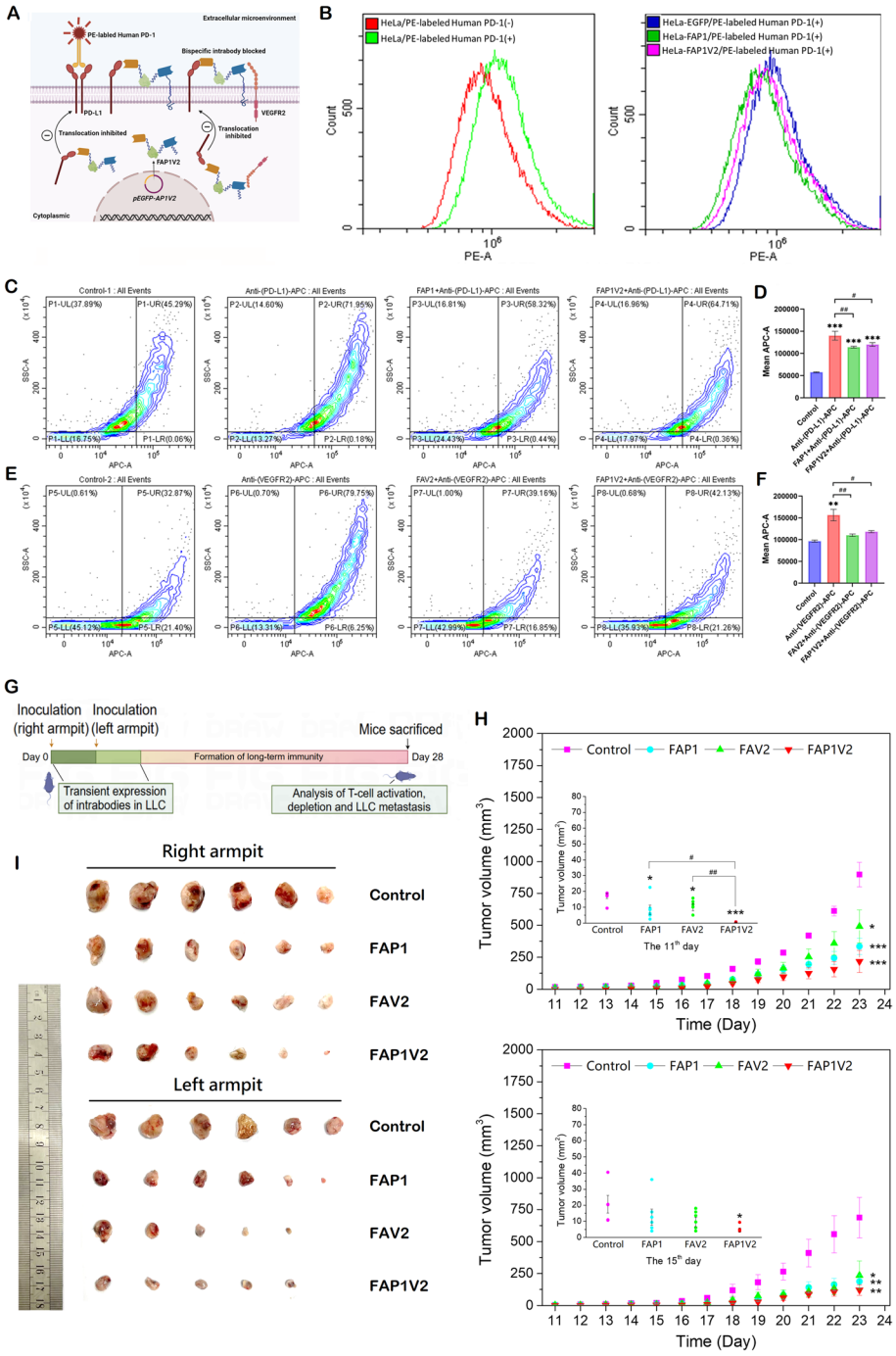

Fig. 3 (See legend on previous page.)

Immunofluorescent microscopy was performed to analyze the recruitment of TCR β high-expressing (TCR β^{hi}) T-cells and PD-1 high-expressing (PD-1^{hi}) immune cells within the tumors. Tumors from the FAP1, FAV2, and FAP1V2 groups exhibited increased infiltration of T cells with high TCR β expression, as well as elevated tumor cell elimination, with the AP1V2 treatment group showing the most pronounced effect (Fig. 4A to D).

In the tumors from the FAP1V2 dual-targeting intrabody treatment group, there were almost no immune cells with high expression of PD-1. In the FAP1 treatment group, there were a few immune cells expressing high levels of PD-1, while the FAV2 treatment group recruited

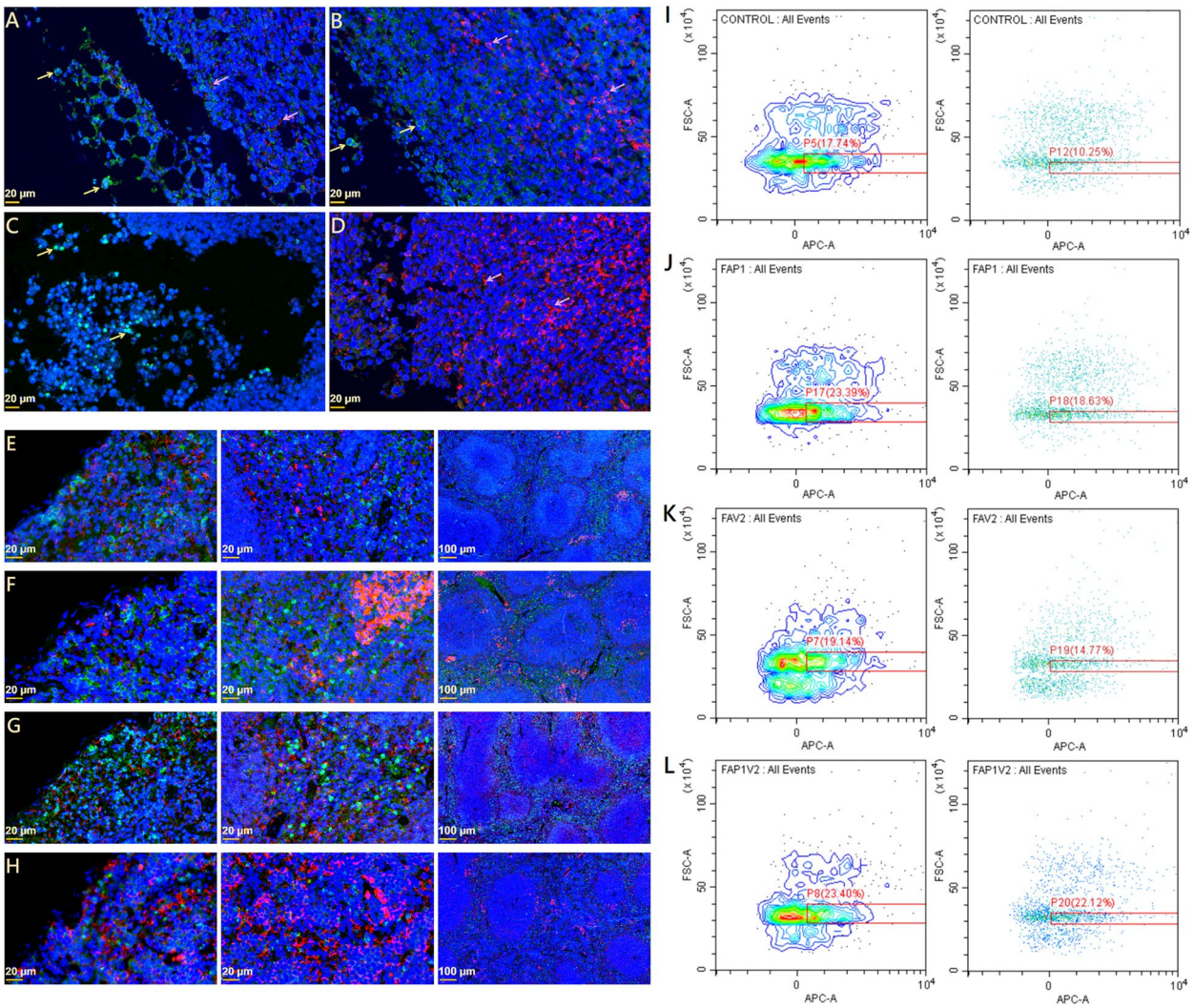

Fig. 4 Immunofluorescence and flow cytometric analysis of intrabody-induced immune system activation against LLC tumors. **A-H** Immune fluorescence analysis of the infiltration of activated T cells (TCR β^{hi}) and immune cells overexpressing PD-1 into the tumor. The tumors were formed by LLC cells transiently expressed the intracellular antibody (**A**) FAP1, (**B**) FAV2, or (**C**) FAP1V2. **D** Control tumors formed by LLC which transiently expressed EGFP but did not express the intrabody. Green fluorescence (indicated by yellow arrows representing TCR β) reveals the distribution of activated T cells, while red fluorescence (indicated by pink arrows representing PD-1) tracks the recruitment and distribution of immune cells exhibiting high levels of PD-1 expression in tumor tissues. **E** to (**H**) Distribution of activated T-cells (antibody labeled with Alexa Fluor488) and PD-1^{hi} immune cells (antibody labeled with CY3) in the marginal and central regions of the spleens in mice bearing LLC tumors expressing single-chain intrabody. The spleens were harvested from mice bearing LLC cells that transiently expressed (**E**) FAP1, **F** FAV2, **G** FAP1V2, or served as (**H**) a control with only EGFP transiently expression, respectively. **I to** (**L**) Flow cytometry detection and analysis of the changes in the proportion of $CD25^{hi}$ immune T cells in the spleen of mice 24 days after the first inoculation of tumor cells transiently expressed intracellular antibodies. The left panel gate shows the total population of $CD25^{hi}$ T cells, while the right panel gate displays a population predominantly consisting of small-sized $CD25^{hi}$ T cells

more PD-1 overexpressing immune cells than the former. However, in the tumor tissue which did not transiently express intrabody, PD-1^{hi} immune cells invaded the tumor tissue much more; few TCR β^{hi} T cells and more tumor cells were detected in this group (Fig. 4D). Overall, tumor tissues that early expressed single-chain antibodies of PD-L1, including FAP1V2 and FAP1, more effectively recruit TCR β^{hi} T cells rather than PD-1^{hi} immune cells, suggesting that along with high expressing of TCR β, activation of T cells and the specificity of the immune response may lead to specific immune inhibition on LLC tumors.

Interestingly, mice inoculated with LLC tumor cells transiently expressing the intrabodies exhibited increased

TCR β^{hi} T cell production in the spleen. Conversely, the control and FAV2 groups displayed much highest levels of PD-1^{hi} immune cells in the spleen (Fig. 4E-H). These findings suggest that transient expression of intrabodies, particularly the dual-specific intrabody FAP1V2 followed by the PD-L1-targeting intrabody FAP1 in LLC tumor cells, significantly enhances the immune response against these tumors, as reported by the activation of T cells.

As a place for activating T cells and as a reservoir for T cells, spleen plays a crucial role in T cell activation, storage, and immune response. Because CD25 (IL-2 receptor alpha chain) is highly expressed on activated T-cells, we determined $CD25^{hi}$ T cells which might vary in the spleen from mice groups with transient expression of the intrabodies. According to the Fluorescence Intensity-Forward scatter area (FSC-A) curve resulting from flow cytometry analysis of the spleen lymphocytes (mainly comprising B and T cells), the immune cells expressing mid-to-high levels of CD25 increased in number in all groups expressing intrabodies, among which the FAP1V2 and FAP1 groups demonstrated the greatest growth, with an increase from 17.7% to 23.4%. $CD25^{hi}$ T cells with relatively smaller sizes remarkably increased in number for all the treatment groups, in which the FAP1V2-transiently expressing group enhanced much more, which was 2.2 folds of that in the control group (Fig. 4I-L). As CD25, which high levels of TCR ligands can induce, is highly expressed on activated T-cells (mainly Teff and Treg cells) and represents active immune regulation and immune response [56], together with the increased generation of TCR β^{hi} T cells, these results further demonstrated enhanced immune response in the FAP1V2-transiently expressing groups. Meanwhile, the increased number of smaller $CD25^{hi}$ T cells (which may be more permeable through tumor tissues) in spleen lymphocytes may imply body systematic regulation and optimization during anticancer immune response. The elevation of CD25 is associated with several physiological effects, one of which involves its association with the IL-2Rβ and IL-2Rγ chains to form a complete IL-2 receptor complex [57], which transmits IL-2 signals to the T-cell, leading to cell activation and proliferation, and consequently directing tumor suppression mechanisms.

FAP1V2 and FAV2 inhibited cancer cell migration

The cell viability analysis indicated that FAP1, FAV2, and FAP1V2 had no obvious impact on the tumor cell viability (Fig. 5A). In HeLa or LLC cells, those expressing FAV2 or FAP1V2 showed the most significant inhibition of cell migration ability, as compared with the non-transfected cells (Fig. 5B). FAP1 expression inhibited cell migration to some degree which is weaker compared to FAV2 or FAP1V2 expression (Fig. 5B). Therefore, we propose that intrabodies FAP1V2 and FAV2 primarily inhibit cancer cell migration by blocking VEGFR2, a key regulator of cell migration, rather than inhibiting cell viability.

In vivo analysis indicated that intact LLC tumor cells in the mice live tissues were not detectable in the FAV2 or FAP1V2 (anti-VEGFR2) intrabodies group. In FAP1 (anti-PD-L1) and the control group (without transient expression of the intrabodies), similar migration in the livers was observed (Fig. 5D). In lung tissues, intact LLC tumor cells were not detected in the FAP1V2 group. The migration was most severe in the control group, followed by the FAP1 group, and then the FAV2 group (Fig. 5E). The results indicated that FAP1V2 as a dual-functional intrabody, could effectively inhibit migration of LLC cells in the test model mice. The binding of vascular endothelial growth factor (VEGF) to VEGFR2 triggered the formation of VEGFR2 receptor dimers and the activation of downstream signaling pathways, playing a crucial role in angiogenesis, vascular development, and cancer metastasis. Consequently, the direct inhibition of VEGFR2 by FAP1V2 resulted in the suppression of cancer metastasis.

FAP1V2-mediated differential gene expression in HeLa cells

To date, there is a lack of information regarding the regulation of genome transcription by an intrabody, particularly those based on V_H domains. With the aim to better understand how the FAP1V2 V_H regions impact signaling pathways, we conducted a transcriptomic

(See figure on next page.)

Fig. 5 The migration ability of cancer cells expressing different V_H intrabodies. **A** MTT assays indicated that the expression of single-chain antibody genes did not significantly impact cell viability in vitro. **B** Migration images of HeLa and LLC cells transiently transfected with different single-chain antibody genes at various time points (showing effective expression of exogenous genes) in scratch assays. The orange box represents the unhealed area. The black dashed lines indicate the edge lines of adherent cells; the green double arrows indicate the distance between the edge lines. **C** Schematic diagrams showing the inhibitory effects of the intrabodies against HeLa and LLC cell migration in scratch assays. The cells without transfection (HeLa-Blank or LLC-Blank) and the cells transfected only with vector plasmids (HeLa-EGFP or LLC-EGFP) were used as controls. *, **, *** represent significant differences compared to the control group at the levels of $P < 0.05$, $P < 0.01$, $P < 0.001$, respectively. **D** Invasion of LLC tumor cells (in mice models) transiently expressing single-chain intrabody to mouse liver tissues. VEGFR2 was determined as a tumor cell biomarker protein. **E** Invasion of LLC cells transiently expressing V_H intrabody to mice lung tissues. Lung sections were from mice inoculated with LLC tumor cells which transiently expressed *FAP1* (a), *FAV2* (b), *FAP1V2* (c) and those transfected with vector plasmid (d)

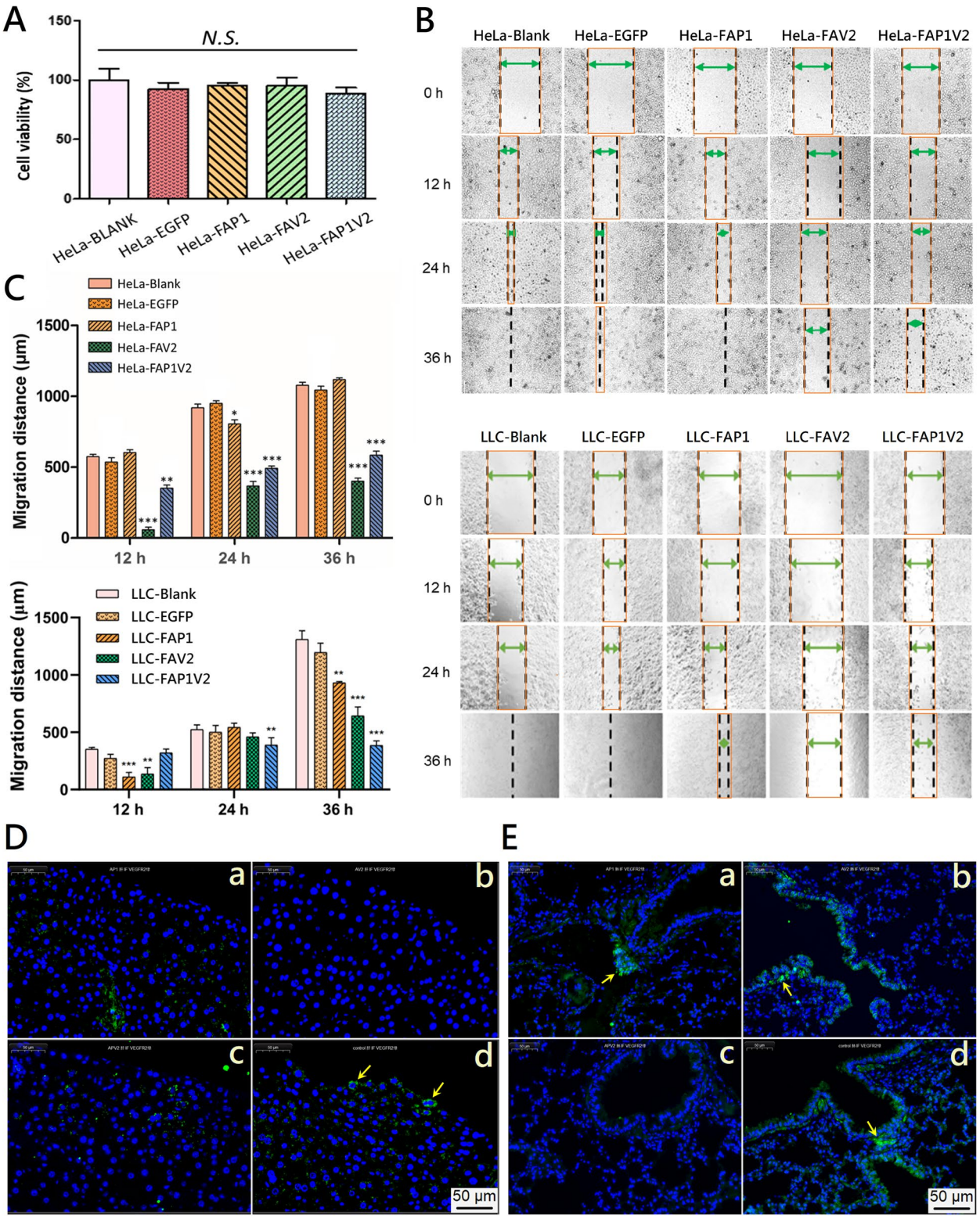

Fig. 5 (See legend on previous page.)

analysis comparing gene expression on transcription level in HeLa-FAP1V2 cells and HeLa-EGFP (control) cells, which were used as PD-L1^{hi}-VEGFR2^{hi} human model cells for in vitro analysis in this study. Our analysis revealed significant differences in gene transcription patterns between the two groups.

Through Gene Ontology (GO) analysis, we identified that genes related to cell migration, cell adhesion, tissue development (such as *PCDH* family, *UCN*, *EGFR-AS1*, *CAMSAP3*, *MXRA8*, *COL8A2*, *ARC*, *DDR2*, *AMH*), cell proliferation, differentiation (including *STIMATE*, *TBX-6*, *INHBA*, *CEMP1*, *PI16*, *SLX1B*, *SPRED3*, *HTR6*, *GSTM2*, *HECW1*, *H2BC4*, *HOXA10-AS*, ENSG00000263809, *H4C15*), and immune system processes (such as *CD160*, *EBI3*) were significantly altered in the HeLa-FAP1V2 group.

Figure 6 illustrates the GO enrichment analysis of the top 37 genes exhibiting significant differential transcription level. Among them, 26 genes like *PCDHA6*, *PCDH1*, *UCN*, *EGFR-AS1*, and *CD160* related to cell migration and immune system response, were significantly upregulated, while 11 genes including *DDR*, *HOXA10-AS*, and *PI16* important for cell migration and adhesion, respectively, were downregulated.

In Fig. 6 and Table 2, we highlighted the signaling pathways linked to the major differentially expressed genes, such as Wnt/β-catenin, ERK1/2, TNFβ, PI3K/AKT, and mTOR signaling pathways. Interestingly, we observed a significant upregulation of CD160 in HeLa-FAP1V2 cells, which plays a crucial role in regulating the immune system by activating natural killer cells and inhibiting T cells [58]. Additionally, the Wnt/β-catenin signaling pathway, known to promote cancer cell migration [59, 60], was inhibited. These signaling changes may play a critical role in immune system activation and inhibition of cell migration caused by FAP1V2 expression in HeLa cells. These pathways may be downstream of the inactivation of PD-L1 and VEGFR2 through intrabody blockage.

Notably, serial genes associated with cell migration were downregulated (Supplementary Fig. 3). Recent studies have shown that as a separate cell migration-related pathway, MET communicates with PI3K to drive cell migration [61]. Through transcriptome sequencing and quantitative analysis, we found that FAP1V2 mediated dual-specific inhibition of VEGFR-2.

and PD-L1 significantly downregulated the transcription level of *MET*, as well as *PIK3CA* (encoding P110α, a major catalytic subunit of PI3K) (Supplementary Fig. 3). Therefore, FAP1V2 can inhibit MET-PI3K signaling which is necessary for cell migration. Furthermore, MET is activated by hepatocyte growth factor (HGF) [62], and transient expression of FAP1V2 reduced *HGF* level to 0 TPM (Supplementary Fig. 3), which suggested suppression of the MET-mediated cell migration and invasion-related pathways, such as interruption of the Met/β1 integrin complex formation which promotes adhesion of cancer cells to the extracellular matrix and plays a crucial role in cancer cell invasion [63].

In primary glioblastoma, MET overexpression was associated with STAT4/PD-L1 signaling activation [64]. Studies have shown that MET amplification inhibited the STING pathway, weakening the effectiveness of immunotherapy [65]. This suggests that MET and PD-L1 may play important roles in tumor immune suppression simultaneously. In our study, the *STAT4* level was significantly downregulated to 50% of the control (Supplementary Fig. 3), while PD-L1 was blocked, leading to downregulated transcription of MET, which collectively contributed to tumor immune activation.

Furthermore, significant downregulation of the gene transcription levels of Matrix metalloproteinases (MMPs), including *MMP1*, *MMP12*, and *MMP13* (Supplementary Fig. 3). Genes expression of microtubule affinity regulating kinase genes MARK1 and MARK2, which influence cell movement and positioning by altering the organization and connections of microtubules, were also downregulated. It was also known that MMPs can disrupt tissue barriers by degrading the extracellular matrix, and can regulate various cellular signaling pathways, potentially contributing to tumor growth, migration, and metastasis, differentiation, and apoptosis [66–68]. *MARK1* and *MARK2* have been found to significantly influence cancer cell migration [69]. *MARK2* exhibits frequent disruptions at both the DNA and RNA levels, which can lead to the acquisition of oncogenic properties such as increased survival and anchorage-independent growth [70]. These results suggest that FAP1V2 not only has the ability to inhibit cancer cell migration and invasion but also has potential to suppress the acquisition of malignant properties by cancer cells.

The impact of dual-targeting intracellular antibodies on transcription of oncogenes

Compared to the HeLa cell line that does not express intracellular antibodies (control), the majority of oncogenes in the cell population expressing dual-target intracellular antibodies exhibited transcription levels comparable to the control. Only four oncogenes—*HGF*, *HIC1*, *CDH1*, and *ESR1*—were significantly downregulated below 70% of the control levels. Conversely, four genes—*JUN*, *RUNX3*, *ROS1*, and *FHIT*—were significantly upregulated, with transcription levels ranging from 1.3 to 2.3 times that of the control.

Among the significantly downregulated oncogenes, hepatocyte growth factor (HGF) is a signaling molecule that activates the MET receptor, promoting cancer cell

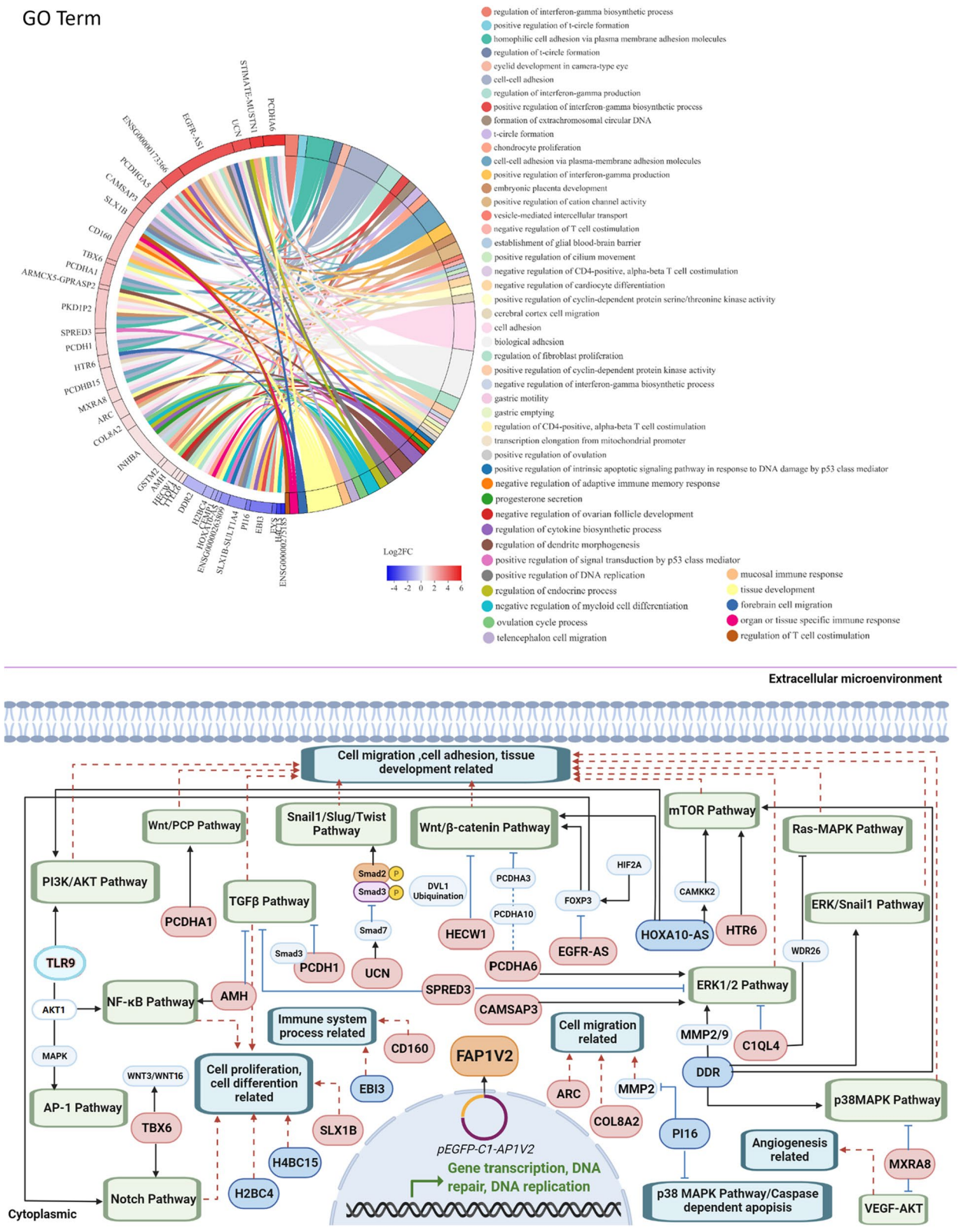

Fig. 6 Analysis of HeLa-FAP1V2 cell transcriptome. **A** This figure shows Circos chord diagrams of the genes with most significantly differential expression. HeLa-EGFP cells were the control. The genes were annotated by GO term. **B** Signal regulation of HeLa cells by FAP1V2. Signaling pathways involve the major differentially expressed genes in transcriptional modulation

Table 2 Transcriptome analysis of differentially expressed genes (DEGs) as representatives in transcriptional modulation

Gene id	Gene name	FC(AP1V2/C1)	*P* value	P adjust	Regulate	C1	AP1V2
ENSG00000142208	*AKT1*	1.010756650	6.69174935E-01	1.000000000	no change	83.48	85.85
ENSG00000104899	*AMH*	2.101739676	3.12064230E-07	0.000036197	up	2.6	5.67
ENSG00000245148	*ARAP1-AS2*	5.899645768	5.27901852E-03	0.111896010	up	0.08	0.46
ENSG00000198576	*ARC*	2.372215767	6.44440346E-06	0.000515077	up	0.79	1.9
ENSG00000186897	*C1QL4*	2.026849060	1.49343911E-04	0.007083502	up	1.33	2.74
ENSG00000110931	*CAMKK2*	0.975856404	5.77199240E-01	1.000000000	down	14.92	14.13
ENSG00000076826	*CAMSAP3*	7.814357821	5.44558913E-04	0.020045584	up	0.03	0.39
ENSG00000117281	*CD160*	4.406592756	4.22929963E-04	0.016352214	up	0.17	1.08
ENSG00000171812	*COL8A2*	2.353187298	4.05983044E-04	0.015787536	up	0.32	0.76
ENSG00000237775	*DDR1-DT*	0.659336441	5.13149552E-01	1.000000000	down	0.1	0.07
ENSG00000162733	*DDR2*	0.495087739	3.38570175E-04	0.013692681	down	0.54	0.23
ENSG00000107404	*DVL1*	1.073618863	5.99012786E-03	0.122558218	up	75.42	81.55
ENSG00000105246	*EBI3*	0.186056139	3.18038016E-04	0.013062599	down	1.4	0.26
ENSG00000146648	*EGFR*	0.972867788	2.05135767E-01	1.000000000	down	27.04	27.12
ENSG00000224057	*EGFR-AS1*	23.618896513	4.54819516E-04	0.017287701	up	0	0.28
ENSG00000170345	*FOS*	1.065223220	1.20666651E-03	0.037082683	up	281.32	292.03
ENSG00000049768	*FOXP3*	2.930384183	3.17040059E-01	1.000000000	up	0.06	0.09
ENSG00000213366	*GSTM2*	2.137829891	3.34931512E-07	0.000038701	up	2.58	5.76
ENSG00000180596	*H2BC4*	0.464377821	4.35290049E-04	0.016702363	down	9.52	4.38
ENSG00000270276	*H4C15*	0.073754054	7.65360114E-32	0.000000000	down	6.9	0.76
ENSG00000002746	*HECW1*	2.045739901	9.30636233E-06	0.000707470	up	4.07	9.88
ENSG00000253187	*HOXA10-AS*	0.365077289	1.33520870E-04	0.006464413	down	4.35	1.67
ENSG00000158748	*HTR6*	2.656881659	9.12827422E-06	0.000696550	up	0.43	1.15
ENSG00000122641	*INHBA*	2.148948401	9.87679508E-04	0.031938481	up	0.28	0.71
ENSG00000177606	*JUN*	1.333945243	1.17391641E-14	0.000000000	up	26.39	36.54
ENSG00000171223	*JUNB*	1.191014653	7.84853730E-22	0.000000000	up	209.92	253.3
ENSG00000130522	*JUND*	0.909652195	1.05063650E-02	0.185063336	down	81.47	77.09
ENSG00000169032	*MAP2K1*	1.005906018	8.72022312E-01	1.000000000	up	39.37	43.37
ENSG00000076984	*MAP2K7*	1.073743731	1.34210557E-01	0.998620043	up	19.46	24.57
ENSG00000073803	*MAP3K13*	1.076345786	2.57402714E-01	1.000000000	up	145.3	121.76
ENSG00000236682	*MAP3K2-DT*	0.792105386	7.45624592E-02	0.690573592	down	23.31	20.64
ENSG00000085511	*MAP3K4*	0.929430316	2.12023621E-01	1.000000000	down	9.93	13.33
ENSG00000156265	*MAP3K7CL*	0.805855650	3.57562421E-01	1.000000000	down	3.08	1.53
ENSG00000104814	*MAP4K1*	2.441986819	1.12348743E-01	0.893253494	up	0.48	0.4
ENSG00000231312	*MAP4K3-DT*	1.307552156	4.43486603E-02	0.490763795	up	3.76	5.24
ENSG00000185386	*MAPK11*	1.234122371	2.35184257E-03	0.061285300	up	11.86	14.86
ENSG00000259438	*MAPK6-DT*	2.930384183	4.53796485E-02	0.496467267	up	0.39	1.16
ENSG00000119487	*MAPKAP1*	0.963895344	2.24534485E-01	1.000000000	down	50.53	46.77
ENSG00000089022	*MAPKAPK5*	0.978515941	6.70633326E-01	1.000000000	down	33.52	30.36
ENSG00000101367	*MAPRE1*	0.905643892	1.51709300E-04	0.007167674	down	79.76	73.21
ENSG00000183019	*MCEMP1*	1.000000000	1.00000000E + 00	1.000000000	no change	0	0
ENSG00000087245	*MMP2*	0.979427597	6.23617900E-01	1.000000000	down	21.57	22.49
ENSG00000100985	*MMP9*	1.000000000	1.00000000E + 00	1.000000000	no change	0	0.09
ENSG00000162576	*MXRA8*	2.423898028	7.72471177E-09	0.000001253	up	3.24	8.86
ENSG00000156453	*PCDH1*	2.718037503	1.18876357E-05	0.000865728	up	0.46	1.18
ENSG00000138650	*PCDH10*	1.000000000	1.00000000E + 00	1.000000000	no change	0	0.01
ENSG00000102290	*PCDH11X*	1.476793868	2.69439763E-01	1.000000000	up	0.12	0.18
ENSG00000099715	*PCDH11Y*	1.327137932	1.20703240E-01	0.933376843	up	55.95	65.92
ENSG00000113555	*PCDH12*	1.202208895	6.20915807E-01	1.000000000	up	0.15	0.43

Table 2 (continued)

Gene id	Gene name	FC(AP1V2/C1)	*P* value	P adjust	Regulate	C1	AP1V2
ENSG00000150275	*PCDH15*	1.000000000	1.00000000E + 00	1.000000000	no change	0.18	0
ENSG00000118946	*PCDH17*	1.526241762	5.86345820E-02	0.585805053	up	0.24	0.38
ENSG00000204970	*PCDHA1*	4.013079623	2.12342469E-04	0.009450876	up	0.08	0.34
ENSG00000250120	*PCDHA10*	2.065254937	1.50727417E-03	0.043770838	up	0.49	1.11
ENSG00000249158	*PCDHA11*	1.066188888	7.45037253E-01	1.000000000	up	0.9	1.25
ENSG00000251664	*PCDHA12*	0.705889181	2.55156722E-02	0.343287367	down	1.14	0.81
ENSG00000239389	*PCDHA13*	0.439714668	6.05662084E-02	0.598987360	down	0.18	0.09
ENSG00000081842	*PCDHA6*	41.474704133	1.98817652E-06	0.000189342	up	0	0.25
ENSG00000204963	*PCDHA7*	0.720408138	2.15213652E-01	1.000000000	down	0.4	0.29
ENSG00000204962	*PCDHA8*	0.549057222	1.05320173E-02	0.185138886	down	0.57	0.32
ENSG00000120324	*PCDHB10*	2.195173590	3.74845160E-02	0.445962086	up	0.19	0.42
ENSG00000197479	*PCDHB11*	1.957930765	8.98925300E-02	0.777257759	up	0.14	0.33
ENSG00000120328	*PCDHB12*	1.346351289	5.65220559E-01	1.000000000	up	0.11	0.22
ENSG00000113248	*PCDHB15*	2.441986819	3.84849298E-04	0.015130588	up	0.33	0.81
ENSG00000272674	*PCDHB16*	0.448437579	1.21565003E-01	0.937411894	down	0.19	0.08
ENSG00000255622	*PCDHB17P*	1.000000000	1.00000000E + 00	1.000000000	no change	0	0.06
ENSG00000146001	*PCDHB18P*	2.232673663	6.46477740E-02	0.627286078	up	0.14	0.33
ENSG00000262096	*PCDHB19P*	1.000000000	1.00000000E + 00	1.000000000	no change	0	0.05
ENSG00000112852	*PCDHB2*	1.918344285	2.82732009E-01	1.000000000	up	0.06	0.29
ENSG00000081818	*PCDHB4*	0.542663738	2.62917120E-01	1.000000000	down	0.15	0.08
ENSG00000113209	*PCDHB5*	19.535894552	2.86745025E-03	0.071408457	up	0.04	0.52
ENSG00000113211	*PCDHB6*	1.000000000	1.00000000E + 00	1.000000000	no change	0.08	0
ENSG00000113212	*PCDHB7*	2.441986819	2.61569012E-01	1.000000000	up	0.03	0.09
ENSG00000120322	*PCDHB8*	1.000000000	1.00000000E + 00	1.000000000	no change	0	0.1
ENSG00000204956	*PCDHGA1*	3.209468391	3.31112321E-03	0.079237072	up	0.11	0.36
ENSG00000253846	*PCDHGA10*	1.907075421	1.34046364E-02	0.219778071	up	0.3	0.59
ENSG00000253159	*PCDHGA12*	1.000000000	1.00000000E + 00	1.000000000	no change	0	0.08
ENSG00000081853	*PCDHGA2*	1.000000000	1.00000000E + 00	1.000000000	no change	0	0.06
ENSG00000262576	*PCDHGA4*	0.066903748	8.20819240E-03	0.154832644	down	0.13	0
ENSG00000253485	*PCDHGA5*	11.807095393	1.39022553E-04	0.006677485	up	0.02	0.22
ENSG00000253731	*PCDHGA6*	1.480401698	3.64760604E-01	1.000000000	up	0.1	0.15
ENSG00000253537	*PCDHGA7*	0.461419224	3.77232073E-02	0.447660534	down	0.42	0.15
ENSG00000253767	*PCDHGA8*	2.526421617	1.53437343E-01	1.000000000	up	0.04	0.08
ENSG00000261934	*PCDHGA9*	0.792760938	7.14208958E-01	1.000000000	down	0.09	0.06
ENSG00000254221	*PCDHGB1*	1.001757260	9.97009425E-01	1.000000000	up	0.23	0.12
ENSG00000253910	*PCDHGB2*	1.513343944	3.83773455E-01	1.000000000	up	0.11	0.28
ENSG00000253305	*PCDHGB6*	0.054447867	2.74363523E-03	0.068890682	down	0.13	0
ENSG00000164530	*PI16*	0.195358946	5.53735809E-04	0.020321736	down	0.74	0.3
ENSG00000105808	*RASA4*	1.246351886	6.38686721E-04	0.022737847	up	11.18	15.04
ENSG00000233297	*RASA4DP*	1.218948194	4.69614198E-01	1.000000000	up	2.33	4.25
ENSG00000111344	*RASAL1*	1.781213915	5.04747712E-02	0.532151811	up	0.39	1.01
ENSG00000075391	*RASAL2*	0.938629750	2.46392078E-01	1.000000000	down	4.32	4.48
ENSG00000100302	*RASD2*	5.860768365	5.03484290E-02	0.532950113	up	0.02	0.11
ENSG00000165105	*RASEF*	1.067965749	6.82245514E-01	1.000000000	up	1.12	1.64
ENSG00000113319	*RASGRF2*	0.596780381	2.15161940E-02	0.306183062	down	0.54	0.25
ENSG00000172575	*RASGRP1*	0.792247632	4.74315278E-01	1.000000000	down	0.66	0.31
ENSG00000068831	*RASGRP2*	0.195358946	8.42289709E-02	0.748011461	down	0.53	0.03
ENSG00000152689	*RASGRP3*	1.300639749	4.71580069E-01	1.000000000	up	0.49	1.45
ENSG00000171777	*RASGRP4*	0.201463913	9.43842008E-02	0.795018489	down	0.12	0.03

Table 2 (continued)

Gene id	Gene name	FC(AP1V2/C1)	*P* value	P adjust	Regulate	C1	AP1V2
ENSG00000270885	*RASL10B*	0.811904608	1.02164587E-03	0.032792130	down	11.66	9.2
ENSG00000122035	*RASL11A*	1.354192691	1.22772829E-01	0.944085552	up	1.38	3.28
ENSG00000103710	*RASL12*	1.000000000	1.00000000E+00	1.000000000	no change	0	0.11
ENSG00000281358	*RASSF1-AS1*	0.666014609	1.97115803E-01	1.000000000	down	2.72	1.83
ENSG00000181625	*SLX1B*	6.185361675	1.85855260E-10	0.000000040	up	0.81	4.27
ENSG00000188766	*SPRED3*	2.890498398	6.49260475E-04	0.023060151	up	0.16	0.65
ENSG00000213533	*STIMATE*	0.935214775	3.90334291E-01	1.000000000	down	6.82	7.16
ENSG00000267280	*TBX2-AS1*	3.581580668	3.05963649E-02	0.387980327	up	0.62	1.26
ENSG00000135111	*TBX3*	1.052276669	4.75400796E-01	1.000000000	up	6.55	8.05
ENSG00000149922	*TBX6*	4.151377592	5.54516152E-07	0.000061051	up	0.42	1.77
ENSG00000239732	*TLR9*	1.000000000	1.00000000E+00	1.000000000	no change	0.04	0
ENSG00000163794	*UCN*	24.498011768	3.44759051E-04	0.013869007	up	0	1.37
ENSG00000145040	*UCN2*	0.513364763	1.49725205E-04	0.007096039	down	4.34	2.25
ENSG00000178473	*UCN3*	1.000000000	1.00000000E+00	1.000000000	no change	0	0
ENSG00000162923	*WDR26*	1.058814227	3.92190573E-02	0.456920471	up	39.24	38.05
ENSG00000125084	*WNT1*	0.976794728	9.81267740E-01	1.000000000	down	0.06	0.12
ENSG00000085741	*WNT11*	0.651196485	1.15378448E-01	0.908884326	down	1.95	1.28
ENSG00000002745	*WNT16*	0.300552224	2.24465511E-02	0.313682925	down	8.78	0.97
ENSG00000108379	*WNT3*	0.924466439	4.77701468E-01	1.000000000	down	3.36	3.15
ENSG00000114251	*WNT5A*	0.917217035	2.64525305E-09	0.000000466	down	210.1	187.79
ENSG00000075290	*WNT8B*	5.860768365	5.03484290E-02	0.532950113	up	0.03	0.19
ENSG00000263809	novel protein gene	0.281828153	5.18096376E-04	0.019211368	down	0.6	0.17

proliferation, migration, and angiogenesis [71]. Hypermethylated in cancer 1 (HIC1) is a transcription factor that regulates genes involved in cell cycle arrest, apoptosis, and differentiation, suppressing tumorigenesis [72]. Cadherin 1 (CDH1, E-cadherin) is a cell adhesion molecule that mediates cell–cell interactions, maintaining tissue integrity and suppressing tumor invasion and metastasis by promoting cell adhesion and preventing cell migration [73]. Estrogen receptor 1 (ESR1) is a nuclear receptor that binds to estrogen and regulates gene expression involved in cell growth, differentiation, and proliferation, thus promoting or suppressing tumorigenesis depending on the context [74].

Among the upregulated oncogenes, the Jun proto-oncogene (JUN), a subunit of the AP-1 transcription factor often regulating tumor growth, apoptosis and metastasis, is associated with immune cell recruitment [75]. Runt-related transcription factor 3 (RUNX3) regulates genes involved in cell cycle arrest, apoptosis, and differentiation, thereby suppressing tumorigenesis by preventing uncontrolled cell growth; meanwhile, it has a role in immune response by regulating transcription of natural cytotoxicity receptor 1 (NCR1/NKp46), an activating natural killer (NK) cell receptor [76]. ROS proto-oncogene 1 (ROS1) product is a receptor tyrosine kinase as well as a type I integral membrane protein that activates downstream signaling pathways involved in cell growth and survival; a significant increase in survival was observed in ROS1-electrovaccinated mice against tumors, and immune memory was achieved [77]. Fragile histidine triad diadenosine triphosphatase (FHIT) is a tumor suppressor gene that codes for a protein involved in DNA repair and cell cycle control [78].

These results indicate that cancer cells may respond to intracellular antibody expression and adjust their gene transcription patterns, as detected through transcriptome sequencing. Therefore, when implementing dual-target immunotherapy aimed at activating immune responses and inhibiting migration, we can incorporate omics analyses and target the aberrantly expressed tumor-related proteins for regulatory and anti-cancer enhancement studies.

Discussion

In physiology, the PD-1/PD-L1 pathway appears to avoid over activation of the immune system and protect normal tissues from injury [79]. PD-1 is expressed on the surface of all activated T cells [80]. When T cells recognize antigens expressed by the MHC complex on the target cells, inflammatory cytokines are produced, which initiates the inflammatory process. Meanwhile, these cytokines lead to the expression of PD-L1 in tissues, which binds

to PD-1 on the surface of T cells and transmits inhibitory signals, leading to immune tolerance [81]. This is a protective mechanism for normal tissues. However, in some tumors, overexpressed PD-L1 inhibits T cell activity by recruiting Src homology 2 domain-containing protein tyrosine phosphatase (SHP) 1/2 to interact with PD-1 and inhibit TCR signaling [82]. As a result, this leads to escape of tumor cells from recognition by the immune system [83]. The inhibitors of anti-PD-L1 may reactivate the immune response of T cells against tumor cells [84]. Interestingly, it has been reported that PD-L1 upregulates the expressions of Slug, Snail and Twist through the mitogen-activated protein kinase (MAPK)/extracellular signal-regulated kinase (ERK) pathway, proving the association between tumor aggressiveness and anti-tumor immune control [85]. Interfering with PD-L1 binding represents a potential therapeutic strategy for re-establishing effective anti-tumor immunity [60, 84, 86, 87]. It is well known that through angiogenesis the tumor cells receive a steady supply of adequate nutrients and oxygen to grow [35], during which VEGF is a key mediator. There is a positive feedback loop between VEGF and VEGFR2. When VEGF binds VEGFR2 expressed on vascular endothelial cells [88], the tumor cells are stimulated to secrete growth factors that accelerate tumor growth [89]. As demonstrated, the antibodies against VEGFR2 can inhibit angiogenesis, degrade existing blood vessels, and rebalance the tumor microenvironment [11, 42, 90]. The PD-L1 is also regulated by hypoxia-inducible factor-1α (HIF-1α), suggesting a relationship between PD-L1 with neovascularization [91–93]. While the use of bispecific antibodies for cancer therapy is gaining attention, the specific application of PD-L1 and VEGFR2 bispecific V_H intrabodies for tumor targeting has yet to be explored.

The current anti-tumor drugs almost all have side effects to a certain extent, mainly because most of them lack specificity [94–96]. Recent studies have demonstrated the potential of combining PD-1/PD-L1 blockade with anti-angiogenic therapies to enhance anti-tumor efficacy. However, these combinations exhibit notable limitations, including well-known immune-related adverse events and systemic side effects, such as organ inflammation, alongside variable patient response rates, often attributed to their immunogenicity [97, 98]. Additionally, traditional antibodies typically have a short half-life and limited tissue penetration.

In contrast, intrabodies present a novel approach to overcoming these challenges. Intrabodies are engineered biomolecules characterized by high affinity, longer half-lives, low toxicity and negligible immunogenicity, as they lack the immunogenic Fc fragment found in conventional antibodies. Intrabodies can avoid many ethical problems by targeting intracellular antigen proteins without affecting the non-target factors. In addition, bispecific antibodies (BsAbs), or even triple-specific antibodies targeting different epitopes of the same antigen or different antigens, can be designed to improve the efficacy of tumor-targeting treatment [99, 100]. They are specifically designed to penetrate intracellular spaces, significantly reducing recognition by the immune system. Their smaller size and enhanced flexibility allow them to effectively target intracellular proteins, facilitating localized therapeutic action within tumor cells, which can lead to increased specificity and decreased systemic toxicity. Furthermore, intrabodies can circumvent resistance mechanisms commonly encountered with conventional monoclonal antibodies by directly interacting with critical signaling pathways. This unique profile positions intrabodies as a promising alternative or complementary strategy to existing combination therapies, particularly for patients with treatment-resistant tumors [101, 102].

Currently, however, there are no reports regarding intracellular antibodies targeting PD-1/PD-L1. In this work, we constructed ultra-small fused nanobodies with dual-targeting capabilities based on the variable heavy (V_H) chains of different anti-PD-L1 and anti-VEGFR2 antibodies that specifically recognize and bind to their respective antigens. Results from our study confirmed that both pathways are targeted simultaneously in the same cancer cells; while a systemically administered antibody should include other elements (modification of Fc fragment, glycosylation, PEGylation, Chemical Crosslinking, polymerization with other proteins, etc.) to increase the half-life that can cause adverse events [103–105]. We achieved their intracellular expression and target protein blockade in tumor cells, enhancing immune therapy against LLC tumors in mice and suppressing metastasis. These multi-target nanobody genes can also be transferred to engineered bacteria for large-scale production and purification, serving as therapeutic agents that target different cellular sites for antigen blockade. The development and application of these single-chain antibodies could significantly reduce the economic burden on cancer patients. It is essential to ensure the protection and effective delivery of the intrabody gene to the tumor cells and their nuclei for expression during the application of such intrabodies. This necessitates the implementation of additional targeting molecules or ligands, such as surface antibodies, RGD sequence or folic acid [106–108]. In our undergoing projects, the nanoparticles (NPs) carrying extracellular or intracellular nanobodies are being explored for improving the durability of the treatment efficacy on the tumor cells.

As shown by the results of WB, the FAV2 signal detectable by gel separation is weaker compared to FAP1 and FAP1V2. This may reflect the cell's ability to respond

and adapt to transgene expression. Specifically, when the intrinsic protein VEGFR2, which has many important functions, cannot perform its role because of the expression of exogenous intracellular antibodies, the growth pressure will select for cells with suitable expression levels. Thus, cells with growth advantage will dominate the population and be detected as the majority. However, since the elements for expressing the inserted genes on the commercial expression plasmids are optimized, and the cell expressing exogenous intrabodies contain at least one copy of plasmid, AFV2 expressed by the cells demonstrates effective antigen blockade efficacy. This has been validated by experiments including competition with commercial antibodies (Figs. 2F, J and 3E, F), cell migration inhibition assays and in vivo cell metastasis inhibition experiments (Fig. 5).

In this study, the bispecific intrabody FAP1V2 presents a similar Y-shape to traditional antibodies, with a "clip" structure, which may provide space for antigen binding. The putative binding sites obtained by docking with PD-L1 or VEGFR2 molecules are also more present in this "clip". The electrostatic complementation between the fusion V_H region with PD-L1 or VEGFR2 and the "clip" structure on the protein surface may provide stability and facilitate better binding of the antibodies to target antigens. In addition to matching the natural structures of the minimum binding epitopes within the target antigens quickly and effectively, the intrabodies can also recognize the antigen regions with matched amino sequences. These two mechanisms provide the basis for strong interaction between the intrabodies and the antigens. Because of the small sizes and improved movability of the intrabodies as compared with the normal intact antibodies, a novel mode of recognition may exist for epitope-intrabody interaction, which includes potential recognition of new binding sites in the antigens that may promote their interference with the antigens, resulting in the aggregation, destabilization, structure changes, and consequently the blockage and inactivation of the antigens. Meanwhile, the interactions between the intrabodies and the target antigens may prevent transmembrane transportation or secretion of corresponding membrane or secretory proteins and their downstream activities. This may lead to the decreased expression level of PD-L1 and VEGFR2 on the cell surface because of the incorrect folding structure of the proteins during binding with the intrabodies which may become an obstacle that prevents transmembrane transportation, meanwhile, the blockage of PD-L1 or VEGFR2 by the intrabodies could lead to Flow cytometry results showed that the binding ability of commercial antibodies to PD-L1 or VEGFR2 on the cell surface was reduced. This result may be caused by the binding of FAP1V2 to PD-L1 or VEGFR2 in the cytoplasm, leading to blockage of their transmembrane transportation to the cell surface. Alternatively, FAP1V2 with IL-2 transmembrane signal peptide and GPI anchor peptide may be transported to the outer cell membrane and anchored to the cell surface, which allows them to bind and block PD-L1 or VEGFR2 on the cell surface and, consequently, the binding of commercial antibodies to PD-L1 or VEGFR2 is inhibited. In this study, the binding between PD-L1 and PD-1 was blocked, indicating immune inactivation caused by the binding of PD-L1 and PD-1 will be blocked, leading to reactivation of the immune recognition along with department of PD-L1 and PD-1 (Fig. 3). This can be the leading cause of the improved immune inhibition on LLC tumors, during which generation of TCR β^{hi} T-cell were remarkably promoted and the invasion of which to the LLC tumors may effectively inhibit tumor growth, partially by specific killing of the tumor cells, demonstration effectiveness of the immune protection caused by FAP1V2 mediated blockade of PD-L1 (Fig. 4). Meanwhile, the blockage of VEGFR2 by FAP1V2 intrabody induced inhibition of cancer cell migration.

T cell receptor (TCR) is a critical molecule for T cells to recognize antigens, and bind to antigen peptide-MHC complexes, which activate T cells [54]. Activated effector T cells (including both CD4+T helper cells and CD8+cytotoxic T cells) begin to proliferate and migrate to the sites of infection or tumors to execute their immune functions. CD8+cytotoxic T cells kill infected cells by releasing perforin and granzymes, while CD4+helper T cells assist other immune cells by secreting cytokines. TCR β (T cell receptor beta chain) is generally highly expressed in αβ T cell populations (including CD4+T cells and CD8+T cells) that play roles in immune responses and adaptive immunity against tumor cells [54, 55]. In our experiments, mice group bearing LLC tumors transiently expressing dual-target intracellular antibodies were detected with a significantly increased population of TCR β^{hi} T cells within the tumor tissues, meanwhile, remarkably reduced LLC tumor sizes were observed as compared with the other mice groups. The results of this study elucidate how the transient expression of AP1V2 intrabodies in tumors aids in activating the immune system, which is well demonstrated to play a significant role in memory suppression of tumors.

Previous studies have indicated that upon antigen recognition, TCR activation initiates intracellular signaling pathways critical for the expression of CD25 [56]. This activation leads to an increase in Ca^{2+} levels, triggering the activation of NFAT, a transcription factor that further promotes CD25 expression [109]. This finding aligns with our observation of an elevated proportion of $CD25^{hi}$

T cells in the dual-target intracellular antibody-expressing tumor model group. CD25 serves as a subunit of the IL-2 receptor (IL-2R); when expressed on T cell surfaces, it can associate with the IL-2Rβ and IL-2Rγ chains to form a complete IL-2R complex [57]. This complex subsequently activates T cells through the IL-2 signaling pathway and promotes their proliferation. Although the spleen is not a site of T cell production, it plays a crucial role in T cell activation, storage, and immune response. It serves as an important immune organ that monitors the blood for pathogens and damaged cells, facilitating the activation and proliferation of T cells in response to antigens. In addition, the spleen acts as a reservoir for T cells, releasing them when needed to mount an immune response and collaborating with B cells and other immune cells to strengthen the overall immune defense.

By the transcriptome analysis, we found that the genes related to cell migration, cell adhesion, tissue development, cell proliferation, cell differentiation and immune system processes, were mostly differentially expressed between the HeLa cells expressing FAP1V2 and the control HeLa-EGFP group. It is the first time that the V_H based intrabodies were applied for analyzing the transcriptome regulation, which we deem could be more target-specific compared to using inhibitors, miRNA and other non-antibody-based blocking or knockdown technologies due to the specificity of the antibodies [11, 110–112]. Transcriptome regulation by intrabodies offers several advantages in terms of target specificity compared to conventional inhibitors, miRNAs, and other non-antibody-based blocking methods. Firstly, intrabodies are engineered antibodies that can be designed to recognize specific intracellular proteins, allowing for precise modulation of target proteins at a post-translational level. This specificity minimizes off-target effects commonly associated with small molecule inhibitors, which can interact with multiple proteins within a pathway [113]. Secondly, intrabodies can be selectively expressed in specific cell types or tissues, further enhancing their precision in targeting specific cellular contexts, which is more challenging for miRNAs that may impact multiple targets [114–116]. Lastly, intrabodies provide a unique advantage of targeting proteins in their native environment, preserving their spatial and temporal regulation on transcriptome, which is vital for maintaining normal cellular functions and avoiding unintended consequences on the transcriptome. Overall, the use of intrabodies for transcriptome regulation presents a highly targeted approach that can improve therapeutic efficacy and safety profiles in complex biological systems.

Currently, most bispecific antibodies against VEGFR2 and other antigens exist in the form of IgG backbone, which has large molecular sizes and can only target the extracellular antigens [117, 118]. Compared to the above methods for blocking a target, the intrabodies we developed with much smaller sizes and could be expressed both within or outside the cells showed no affection on normal cell viability or proliferation (Supplementary Fig. 1). In addition to the advantages that ensure the cellular and systemic biosafety of intrabodies (as mentioned above) and their effective blockade of target sites, the integration of advanced targeted delivery technologies enables intrabodies to selectively target various tumor tissues, tumor microenvironments, and specific cellular and subcellular locations. This multifaceted approach not only enhances the potential for achieving more precise therapeutic effects in cancer treatment but also underscores the importance of efficient targeting mechanisms for successful in vivo applications. Our laboratory has also been developing various delivery systems, including micelles, liposomes, and polymeric vectors [119], which provide distinct benefits regarding stability, bioavailability, and specificity. Therefore, a comprehensive examination of these delivery strategies, combined with the unique properties of intrabodies, will strengthen their overall potential and effectiveness in vivo, reinforcing the case for their application in targeted cancer therapies. Thus the intrabodies can be developed to potential tools with strong biosafety for in vivo applications and for the exploration of the regulation pathways mediated by the intra or extracellular target tumor-associated-antigens (TAAs) more precisely.

In the significantly upregulated genes, protocadherins (*PCDHs*) (*PCDHA6*, *PCDHGA5*, *PCDHB15*, *PCDH1*, *PCDHA1*) belong to the cadherin family associated with cell adhesion [120]. These transmembrane proteins regulate Wnt/β-catenin [121], Wnt /planar cell polarity (PCP) [122], mTOR signaling pathways, et al. Wnt associated signaling are transduced by at least two distinct pathways: the well-established canonical Wnt/β-catenin pathway and the β-catenin independent noncanonical Wnt pathway (e.g., the Wnt/PCP Pathway). In general, the Wnt signaling pathway is thought to play a key role in tumorigenesis through the canonical Wnt/β-catenin cascade. Noncanonical Wnt/PCP signaling plays an important role in cancer progression, invasion, metastasis, and angiogenesis [123]. Notably, PCDHGC3 negatively regulates Wnt/β-catenin and mTOR signaling [121]. However, in the Wnt/PCP pathway, some PCDHs (PCDH9, PCDHA1, PCDHB3, etc.) act as PCP modulators and are upregulated in some tumor cell lines [122, 123]. It has been reported that PCDH1 combined with SMAD3 can downregulate TGF-β1 [124]. TGF-β1 regulates cell growth and differentiation, and high levels of TGF-β can be detected in most tumor cells. Therefore, some PCDHs (PCDH1, PCDHGC3, etc.) can be used

as candidate tumor suppressors [125]. In this study, the Wnt pathway involved in the significant upregulation of PCDHs in FAP1V2-HeLa cells needs to be further investigated to determine the specific pathway involved in the Wnt factor. Urocortin (UCN) peptide shares structural and functional homology with corticotropin-releasing factor (CRF). Studies have shown that UCN is a potential mediator that inhibits the carcinogenic signaling of TGF-β1 [126]. In addition, UCN modulates tumor angiogenesis and inhibits tumor cell growth by regulating VEGF via CRFR2 [127]. UCN inhibits endometrial cancer cell migration through binding CRFR2, but its expression is downregulated in human endometrial cancer [128, 129]. MXRA8 is a transmembrane protein that can regulate a variety of signaling pathways. Its RGD motif interact with integrin αvβ3 that plays a critical role in angiogenesis, inhibits the migration of endothelial cells, and promotes apoptosis. MXRA8 suppressed the VEGF-induced activation of AKT and p38 MAP kinase in endothelial cells [130, 131]. Epidermal growth factor receptor-antisense RNA1 (*EGFR-AS1*) is an oncogenic long noncoding RNA (lncRNA) recently discovered in several cancers, such as liver cancer. *EGFR-AS1* inhibits FOXP3 expression, which induces epithelial-mesenchymal transformation in NSCLC by stimulating the Wnt/β-catenin signaling pathway [132–134]. UCN, MXRA8 and *EGFR-AS1* were significantly upregulated in HeLa-FAP1V2.

Among the significantly downregulated genes, domain receptor tyrosine kinase 2 (DDR2) is a member of the receptor tyrosine kinase (RTK) family, which is activated by collagen I, II, III and X. Multiple studies have demonstrated that DDR2 is upregulated in many tumor types. It participates in a variety of signaling pathways and promotes tumor progression including tumor angiogenesis, cell adhesion, and matrix remodeling [135–137]. For example, in hepatocellular carcinoma, DDR2 amplification mediates sorafenib resistance through enhancing the NF-κB/C-REL signaling pathway [138]. DDR2 facilitates hepatocellular carcinoma invasion and metastasis via activating ERK signaling and stabilizing Snail1 [139]. DDR2 induces gastric cancer cell activity by activating the mTORC2 signaling pathway [140]. The downregulation of *DDR2* transcription may be important in suppressing cancer cell migration. In addition, studies have shown that targeting DDR2 can enhance tumor response to PD-1 immunotherapy, which provides a strong scientific rationale for targeting DDR2 in combination with PD-1 inhibitors [141]. It should be mentioned that peptidase inhibitor 16 gene (*PI16*), which is localized on chromosome 6p21.2 [142], was downregulated in HeLa-FAP1V2. Hazell GG, e*t al.* found that PI16 overexpression inhibits human coronary artery endothelial cells (HCAECs) migration and secretion of matrix metalloproteinase 2 (MMP2) activity [143], which has long been known to participate in the invasion and migration of Endothelial cells (ECs) during sprouting angiogenesis [144]. Here, we deem that the downregulation of PI16 may be related with the self-adjustability of cancer cells.

The study of genome regulation in cancer cells following the expression of the intrabody enhances our understanding of genome transcription influenced by the transient expression of FAP1V2. It provides insights into the pathways involved in the response to the intrabody and identifies other potential therapeutic targets. Given that protein expressions involve indirect factors—such as post-transcriptional modifications and degradation, intracellular antigen accumulation and/or degradation (such as possible ubiquitination), and transport capabilities of antigens—beyond gene transcription regulation. In this regard, our laboratory is currently investigating how intracellular antibodies influence regulatory networks and mechanisms at the post-transcriptional levels.

Conclusions

In this work, we developed a novel bispecific V_H-based intrabody, FAP1V2, for tumor-targeting immune therapy based on checkpoint-blockade combining metastasis inhibition and investigated the regulation of FAP1V2 on genome expression at the transcriptome level. The bispecific intrabody, FAP1V2 targeting and blocking of both intracellular or extracellular PD-L1 and VEGFR2 was constructed, which inhibited their biological functions and downstream responses. As the consequence of its inhibition on the binding of PD-1 (highly expressed by "inactivated" immune cells) to PD-L1, the PD-1/PD-L1 checkpoint was blocked. TCR β^{hi} T-cell mediated specific immune inhibition of LLC tumors was greatly enhanced in both first- and secondary tumors which were formed by LLC cells that had transiently expressed FAP1V2 intrabody. Metastasis of the tumor cells was inhibited by FAP1V2. Relevant factors associated with Wnt/β-catenin, TGF-β1 and PI3K/AKT signaling pathways were analyzed in HeLa cells transiently expressing FAP1V2. PCDHs, UCN and MXRA8 factors that suppress cancer cell migration were upregulated, and MET, PI3K 110α, DDR2 and PI16 that promote cancer cell migration were downregulated. This study presents a potential strategy for enhancing immune activation while inhibiting metastasis in tumor therapy. Based on this research, we also achieved enhanced anti-CLC tumor efficacy through AP1V2-NP-mediated immune responses in our laboratory. Lastly, this study introduces a new framework for investigating the intracellular regulation of signaling pathways through the application of V_H intrabodies.

Abbreviations

$(GGGGS)_3$ linker	Glycine-Glycine-Glycine-Glycine-Serine tripeptide linker (repeated three times)
AKT	Protein kinase B
AMH	Anti-Müllerian hormone (also known as Müllerian-inhibiting substance or MIS)
APC	Allophycocyanin
ARC	Activity-regulated cytoskeleton-associated protein
BsAbs	Bispecific antibodies
CAMSAP3	Calcium-modulating ligand of calcineurin 3
CD160	CD160 molecule
CD25	Cluster of differentiation 25
CDH1	Cadherin 1
CEMP1	Centromere protein 1
CLSM	Confocal laser scanning microscopy
co-IP	Co-immunoprecipitation
COL8A2	Collagen, type VIII, alpha 2
C-REL	Protein encoded by *c-Rel* proto-oncogene, NF-kB subunit
CRFR2	Corticotropin-releasing factor receptor 2
DDR2	Discoidin domain receptor 2
EBI3	Epstein-Barr virus-induced gene 3
EC	Endothelial Cell
ECD	Extracellular domain
EGFP	Enhanced green fluorescent protein
EGFR-AS1	Epidermal Growth Factor Receptor Antisense RNA 1
ERK	Extracellular signal-regulated kinase
ESR1	Estrogen receptor 1
FHIT	Fragile histidine triad
FOXP3	Forkhead box protein P3
GO enrichment	Gene ontology enrichment analysis
GPI anchor peptide	Glycosylphosphatidylinositol anchor peptide
GSTM2	Glutathione S-transferase Mu 2
H2BC4	Histone H2B type 4
H4C15	H4 clustered histone 15
HCAEC	Human Coronary Artery Endothelial Cells
HECW1	HECT, C2 and WW domain containing E3 ubiquitin protein ligase 1
HGF	Hepatocyte growth factor
HIC1	HIC ZBTB transcriptional repressor 1
HOXA10-AS	Homeobox A10 antisense RNA
HTR6	5-Hydroxytryptamine receptor 6
IL-2	Interleukin-2
INHBA	Inhibin, beta A
JUN	Jun proto-oncogene
LLC	Lewis Lung Carcinoma
MAPK	Mitogen-activated protein kinase
MARK1	Microtubule affinity-regulating kinase 1
MARK2	Microtubule affinity-regulating kinase 2
MET	Met proto-oncogene product, receptor tyrosine kinase
MMP	Matrix Metalloproteinase
MMP2	Matrix metalloproteinase 2
mTOR	Mechanistic target of rapamycin kinase
MXRA8	Matrix remodelling associated 8
NF-κB	Nuclear factor of kappa light polypeptide gene enhancer in B cells 1
NP	Nanoparticle
p38 MAP kinase	P38 mitogen-activated protein kinase
PCDH	Protocadherin (family of proteins)
PCDH1	Protocadherin 1
PCDHA6	Protocadherin alpha 6
PCDHGC3	Protocadherin gamma subfamily C, member 3
PCP	Planar Cell Polarity or Precursor Cell Population (needs context)
PD-1	Programmed cell death 1
PD-L1	Programmed cell death 1 ligand 1
PE	Phycoerythrin
PI16	Peptidase inhibitor 16
PI3K	Phosphoinositide 3-kinase
PIK3CA	Phosphoinositide-3-kinase catalytic subunit alpha
RBITC	Rhodamine B isothiocyanate
RGD	Arginine-Glycine-Aspartic acid (amino acid sequence)
ROS1	Protein encoded by ROS proto-oncogene 1
RTK	Receptor tyrosine kinase
RUNX3	Runt-related transcription factor 3/RUNX family transcription factor 3
SLX1B	SLX1 homolog B, structure-specific endonuclease subunit
SMAD3	SMAD family member 3/Mothers against dpp (MAD) family member 3
SPRED3	Sprouty-related, EVH1 domain-containing protein 3
STAT4	Signal transducer and activator of transcription 4
STIMATE	Stromal interaction molecule (STIM) activating enhancer
STING	Stimulator of interferon response cGAMP interactor
TAA	Tumor-associated antigen
TBX-6	T-box transcription factor 6
TCR β	T cell receptor beta chain
TGF-β1	Transforming growth factor beta 1
TIL	Tumor-infiltrating lymphocytes
TNFβ	Tumor necrosis factor beta
UCN	Urocortin
VEGFR2	Vascular endothelial growth factor receptor 2
V_H	Variable regions of heavy chain
V_L	Light chain variable region
Wnt	Wingless-type MMTV integration site family

Supplementary Information

The online version contains supplementary material available at https://doi.org/10.1186/s12943-025-02253-6.

Supplementary Material 1.

Supplementary Material 2.

Acknowledgements

The schematic diagrams in Figs. 2 and 3A were created using BioRender.com platform. Fig. 3G was created using Figdraw.com platform. We would like to acknowledge Biwei Ye at Fujian Institute of Research on the Structure of Matter, Chinese Academy of Sciences for assistance with tumor cell inoculation.

Authors' contributions

L.Z. contributed to the conceptualization; L.Z., Y.L., L.H., Y.W., C.H., X. S., S.T., J.C., P.H. and Z.C. contributed to methodology; L.Z., Y.L., L.H. and Y.W. performed Data collection and investigation; L.Z., Y.L., L.H. and Y.W. contributed to visualization; L.Z. and Z.C. contributed to funding acquisition; L.Z. and Z.C. were responsible for project administration; L.Z. and Z.C. contributed to supervision; L.Z., Y.L., L.H. and Y.W. prepared the figures; L.Z. and Y.L. wrote the original draft, and L.Z., L.H., Z.C., Z.-F. Ke, and Z.-S.C. reviewed and edited the manuscript. All authors reviewed the manuscript.

Funding

This work was financially supported by National Natural Science Foundation of China (21877113, 82173744), Fujian Province Guiding Project (2024Y0051), Key Project of Fujian Provincial Natural Science Foundation (2024J02027), Natural Science Foundation of Fujian Province (2020l0036), National Key Research and Development Program of China (2022YFB3503700), Self-deployment Project Research Program of Haixi Institutes, Chinese Academy of Sciences (No. CXZX-2022-GH10).

Data availability

The V_H sequences of the anti-PD-L1 antibody (durvalumab-VH, PDB: 5XJ4_H) and the anti-VEGFR2 antibody (GenBank: ACH41918.1), respectively, were retrieved from the publicly available National Center for Biotechnology Information (https://www.ncbi.nlm.nih.gov/) database.

Declarations

Ethics approval and consent to participate

The protocol was approved by the Animal Ethics Committee of Fujian Institute of Research on the Structure of Matter, Chinese Academy of Sciences. The research strictly adhered to the Declaration of Helsinki, the International Ethical Guidelines for Biomedical Research formulated by the World Health

Organization, the Regulations on the Management of Experimental Animals issued by the former State Science and Technology Commission of the People's Republic of China, the Guiding Opinions on the Humane Treatment of Experimental Animals issued by the Ministry of Science and Technology, and the relevant regulations of the National Natural Science Foundation of China.

Consent for publication
Not applicable.

Competing interests
The authors declare no competing interests.

Author details
[1]State Key Laboratory of Structural Chemistry, Fujian Institute of Research on the Structure of Matter, Chinese Academy of Sciences, Fuzhou 350108, China. [2]University of Chinese Academy of Sciences, Beijing 100049, China. [3]College of Life Sciences, Fujian Agriculture and Forestry University, Fuzhou 350002, China. [4]National Engineering Research Center for Sugarcane, Fujian Agriculture and Forestry University, Fuzhou 350002, China. [5]College of Pharmacy and Health Sciences, St. John's University, Queens, NY 11439, USA. [6]Department of Pathology, The First Affiliated Hospital, Sun Yat-Sen University, Guangzhou, Guangdong Province, P.R. China.

Received: 4 November 2024 Accepted: 30 January 2025
Published online: 19 April 2025

References

1. Zhang L, Ye B, Chen Z, Chen Z-S. Progress in the studies on the molecular mechanisms associated with multidrug resistance in cancers. Acta Pharm Sin B. 2023;13:982–97.
2. Gottesman MM. Mechanisms of cancer drug resistance. Annu Rev Med. 2002;53:615–27.
3. Holohan C, Van Schaeybroeck S, Longley DB, Johnston PG. Cancer drug resistance: an evolving paradigm. Nat Rev Cancer. 2013;13:714–26.
4. Wherry EJ. T cell exhaustion. Nat Immunol. 2011;12:492–9.
5. Pauken KE, Wherry EJ. SnapShot: T Cell Exhaustion. Cell. 2015;163:1038-U299.
6. Wherry EJ, Kurachi M. Molecular and cellular insights into T cell exhaustion. Nat Rev Immunol. 2015;15:486–99.
7. Stone ML, Lee J, Lee JW, Coho H, Tariveranmoshabad M, Wattenberg MM, et al. Hepatocytes coordinate immune evasion in cancer via release of serum amyloid A proteins. Nat Immunol. 2024;25:755–63.
8. Sharma P, Allison JP. The future of immune checkpoint therapy. Science. 2015;348:56–61.
9. Fang HP, Guo ZP, Chen J, Lin L, Hu YY, Li YH, et al. Combination of epigenetic regulation with gene therapy-mediated immune checkpoint blockade induces anti-tumour effects and immune response *in vivo*. Nat Commun. 2021;12:6742.
10. Chang TG, Cao YY, Sfreddo HJ, Dhruba SR, Lee SH, Valero C, et al. LORIS robustly predicts patient outcomes with immune checkpoint blockade therapy using common clinical, pathologic and genomic features. Nat Cancer. 2024;5:1158–75.
11. Matsukane R, Watanabe H, Hata K, Suetsugu K, Tsuji T, Egashira N, et al. Prognostic significance of pre-treatment ALBI grade in advanced non-small cell lung cancer receiving immune checkpoint therapy. Sci Rep. 2021;11:15057.
12. Patterson A, Auslander N. Mutated processes predict immune checkpoint inhibitor therapy benefit in metastatic melanoma. Nat Commun. 2022;13:5151.
13. Robertson AG, Meghani K, Cooley LF, McLaughlin KA, Fall LA, Yu YN, et al. Expression-based subtypes define pathologic response to neoadjuvant immune-checkpoint inhibitors in muscle-invasive bladder cancer. Nat Commun. 2023;14:2126.
14. Lozano AX, Chaudhuri AA, Nene A, Bacchiocchi A, Earland N, Vesely MD, et al. T cell characteristics associated with toxicity to immune checkpoint blockade in patients with melanoma. Nat Med. 2022;28:353–62.
15. Torres ETR, Ho WJ, Danilova L, Tandurella JA, Leatherman J, Rafie C, et al. Entinostat, nivolumab and ipilimumab for women with advanced HER2-negative breast cancer: a phase Ib trial. Nat Cancer. 2024;5:866–79.
16. Uson PLSU, Bekaii-Saab T. Moving beyond single-agent checkpoint inhibition in biliary tract cancers: what is the next frontier? Immunotherapy. 2023;15:531–40.
17. Hilton JF, Ott PA, Hansen AR, Li ZJ, Mathew M, Messina CH, et al. INDUCE-2: A Phase I/II, open-label, two-part study of feladilimab in combination with tremelimumab in patients with advanced solid tumors. Cancer Immunol Immun. 2024;73:44.
18. Yarchoan M, Gane EJ, Marron TU, Perales-Linares R, Yan J, Cooch N, et al. Personalized neoantigen vaccine and pembrolizumab in advanced hepatocellular carcinoma: a phase 1/2 trial. Nat Med. 2024;30:1044–53.
19. Petitprez F, Meylan M, de Reyniès A, Sautès-Fridman C, Fridman WH. The tumor microenvironment in the response to immune checkpoint blockade therapies. Front Immunol. 2020;11:784.
20. Gao XY, Ji K, Jia YN, Shan F, Chen Y, Xu N, et al. Cadonilimab with chemotherapy in HER2-negative gastric or gastroesophageal junction adenocarcinoma: the phase 1b/2 COMPASSION-04 trial. Nat Med. 2024;30:1943–51.
21. Zeng TM, Yang G, Lou C, Wei W, Tao CJ, Chen XY, et al. Clinical and biomarker analyses of sintilimab plus gemcitabine and cisplatin as first-line treatment for patients with advanced biliary tract cancer. Nat Commun. 2023;14:1340.
22. Chames P, Van Regenmortel M, Weiss E, Baty D. Therapeutic antibodies: successes, limitations and hopes for the future. Br J Pharmacol. 2009;157:220–33.
23. Agata Y, Kawasaki A, Nishimura H, Ishida Y, Tsubata T, Yagita H, et al. Expression of the PD-1 antigen on the surface of stimulated mouse T and B lymphocytes. Int Immunol. 1996;8:765–72.
24. Keir ME, Butte MJ, Freeman GJ, Sharpel AH. PD-1 and its ligands in tolerance and immunity. Annu Rev Immunol. 2008;26:677–704.
25. Nishimura H, Agata Y, Kawasaki A, Sato M, Imamura S, Minato N, et al. Developmentally regulated expression of the PD-1 protein on the surface of double-negative (CD4-CD8-) thymocytes. Int Immunol. 1996;8:773–80.
26. Dong H, Zhu G, Tamada K, Chen L. B7–H1, a third member of the B7 family, co-stimulates T-cell proliferation and interleukin-10 secretion. Nat Med. 1999;5:1365–9.
27. Zhu X, Lang J. Soluble PD-1 and PD-L1: predictive and prognostic significance in cancer. Oncotarget. 2017;8:97671–82.
28. Dong HD, Strome SE, Salomao DR, Tamura H, Hirano F, Flies DB, et al. Tumor-associated B7–H1 promotes T-cell apoptosis: A potential mechanism of immune evasion. Nat Med. 2002;8:793–800.
29. Inozume T, Hanada KI, Wang QJ, Ahmadzadeh M, Wunderlich JR, Rosenberg SA, et al. Selection of CD8+PD-1+ Lymphocytes in Fresh Human Melanomas Enriches for Tumor-reactive T Cells. J ImmunoTher. 2010;33:956–64.
30. Juneja VR, McGuire KA, Manguso RT, LaFleur MW, Collins N, Haining WN, et al. PD-L1 on tumor cells is sufficient for immune evasion in immunogenic tumors and inhibits CD8 T cell cytotoxicity. J Exp Med. 2017;214:895–904.
31. Yu XB, Gao RL, Li YQ, Zeng CW. Regulation of PD-1 in T cells for cancer immunotherapy. Eur J Pharmacol. 2020;881: 173240.
32. Diskin B, Adam S, Cassini MF, Sanchez G, Liria M, Aykut B, et al. PD-L1 engagement on T cells promotes self-tolerance and suppression of neighboring macrophages and effector T cells in cancer. Nat Immunol. 2020;21:442–54.
33. Grzywnowicz M, Karczmarczyk A, Skorka K, Zajac M, Zaleska J, Chocholska S, et al. Expression of programmed death 1 ligand in different compartments of chronic lymphocytic leukemia. Acta Haematol. 2015;134:255–62.
34. Liu Z, Qi L, Li Y, Zhao X, Sun B. VEGFR2 regulates endothelial differentiation of colon cancer cells. BMC Cancer. 2017;17:593.
35. Carmeliet P, Jain RK. Angiogenesis in cancer and other diseases. Nature. 2000;407:249–57.
36. Carmeliet P. VEGF as a key mediator of angiogenesis in cancer. Oncology. 2005;69(Suppl 3):4–10.
37. Apte RS, Chen DS, Ferrara N. VEGF in signaling and disease: Beyond discovery and development. Cell. 2019;176:1248–64.
38. Carmeliet P, Jain RK. Molecular mechanisms and clinical applications of angiogenesis. Nature. 2011;473:298–307.
39. Zhang Z, Neiva KG, Lingen MW, Ellis LM, Nör JE. VEGF-dependent tumor angiogenesis requires inverse and reciprocal regulation of VEGFR1 and VEGFR2. Cell Death Differ. 2010;17:499–512.

40. Olsson AK, Dimberg A, Kreuger J, Claesson-Welsh L. VEGF receptor signalling - in control of vascular function. Nat Rev Mol Cell Biol. 2006;7:359–71.
41. Chen Z, Xie W, Acheampong DO, Xu M, He H, Yang M, et al. A human IgG-like bispecific antibody co-targeting epidermal growth factor receptor and the vascular endothelial growth factor receptor 2 for enhanced antitumor activity. Cancer Biol Ther. 2016;17:139–50.
42. Zhou HJ, Xu Z, Wang Z, Zhang H, Zhuang ZW, Simons M, et al. SUMOylation of VEGFR2 regulates its intracellular trafficking and pathological angiogenesis. Nat Commun. 2018;9:3303.
43. Niu G, Sun L, Pei Y, Wang D. Oleanolic acid inhibits colorectal cancer angiogenesis by blocking the VEGFR2 signaling pathway. Anticancer Agents Med Chem. 2018;18:583–90.
44. Wang M, Jiang X. SUMOylation of vascular endothelial growth factor receptor 2 inhibits the proliferation, migration, and angiogenesis signaling pathway in non-small cell lung cancer. Anticancer Drugs. 2020;31:492–9.
45. Wang G, Sun M, Jiang Y, Zhang T, Sun W, Wang H, et al. Anlotinib, a novel small molecular tyrosine kinase inhibitor, suppresses growth and metastasis via dual blockade of VEGFR2 and MET in osteosarcoma. Int J Cancer. 2019;145:979–93.
46. Trapnell C, Pachter L, Salzberg SL. TopHat: discovering splice junctions with RNA-Seq. Bioinformatics. 2009;25:1105–11.
47. Robinson MD, McCarthy DJ, Smyth GK. edgeR: a Bioconductor package for differential expression analysis of digital gene expression data. Bioinformatics. 2010;26:139–40.
48. Kolkman J, Law D. Nanobodies - from llamas to therapeutic proteins. Drug Discov Today Technol. 2010;7:e95–146.
49. Zhu ZY, Nie XY, Deng LX, Ding J, Chen JP, Zhu JY, et al. Regulation of cervical cancer via G15-mediated inhibition of G protein-coupled estrogen receptor. Anti-Cancer Drug. 2024;35:817–29.
50. Yabuki Y, Mitsuhashi A, Ogino H, Yoshida A, Nguyen NT, Yoneda H, et al. Hypoxia-inducible factor-targeting therapy augmented the sensitivity to programmed death ligand-1 blockade by enhancing interferon-γ-induced chemokines in tumor cells. Int J Cancer. 2024. Online ahead of print
51. Li J, Wang XH, Li ZL, Li MZ, Zheng XL, Zheng DX, et al. SULF1 Activates the VEGFR2/PI3K/AKT Pathway to Promote the Development of Cervical Cancer. Curr Cancer Drug Tar. 2024;24:820–34.
52. Zhu LN, Zhang YX, Ding JN, Xin WJ, Fan GC, Song ZL, et al. Intelligent DNA Nanosystem for Broad-Spectrum Oncological Typing and Therapy. Acs Sensors. 2024;9:6655–66.
53. Sato M, Maishi N, Hida Y, Yanagawa-Matsuda A, Alam MT, Sakakibara-Konishi J, et al. Angiogenic inhibitor pre-administration improves the therapeutic effects of immunotherapy. Cancer Med-Us. 2023;12:9760–73.
54. Zareie P, Szeto C, Farenc C, Gunasinghe SD, Kolawole EM, Nguyen A, et al. Canonical T cell receptor docking on peptide-MHC is essential for T cell signaling. Science. 2021;372:eabe9124.
55. Kurt RA, Park JA, Panelli MC, Schluter SF, Marchalonis JJ, Carolus B, et al. T-lymphocytes infiltrating sites of tumor rejection and progression display identical V-beta usage but different cytotoxic activities. J Immunol. 1995;154:3969–74.
56. Snook JP, Kim C, Williams MA. TCR signal strength controls the differentiation of $CD4^+$ effector and memory T cells. Sci Immunol. 2018;3:eaas9103.
57. Baan CC, van Riemsdijk-Overbeeke IC, Boelaars-van Haperen MJAM, IJzermans JMN, Weimar W. Inhibition of the IL-15 pathway in anti-CD25 mAb treated renal allograft recipients. Transpl Immunol. 2002;10:81–7.
58. Piotrowska M, Spodzieja M, Kuncewicz K, Rodziewicz-Motowidło S, Orlikowska M. CD160 protein as a new therapeutic target in a battle against autoimmune, infectious and lifestyle diseases. Analysis of the structure, interactions and functions. Eur J Med Chem. 2021;224:113694.
59. Guo Q, Xu J, Huang Z, Yao Q, Chen F, Liu H, et al. ADMA mediates gastric cancer cell migration and invasion via Wnt/β-catenin signaling pathway. Clin Transl Oncol. 2021;23:325–34.
60. Peng Q, Qiu X, Zhang Z, Zhang S, Zhang Y, Liang Y, et al. PD-L1 on dendritic cells attenuates T cell activation and regulates response to immune checkpoint blockade. Nat Commun. 2020;11:4835.
61. Hervieu A, Heuss SF, Zhang C, Barrow-McGee R, Joffre C, Menard L, et al. A PI3K- and GTPase-independent Rac1-mTOR mechanism mediates MET-driven anchorage-independent cell growth but not migration. Sci Signal. 2020;13:eaba8627.
62. Papaccio F, Della Corte CM, Viscardi G, Di Liello R, Esposito G, Sparano F, et al. HGF/MET and the immune system: Relevance for cancer immunotherapy. Int J Mol Sci. 2018;19:3595.
63. Barrow-McGee R, Kishi N, Joffre C, Menard L, Hervieu A, Bakhouche BA, et al. Beta 1-integrin-c-Met cooperation reveals an inside-in survival signalling on autophagy-related endomembranes. Nat Commun. 2016;7:11942.
64. Wang QW, Sun LH, Zhang Y, Wang Z, Zhao Z, Wang ZL, et al. MET overexpression contributes to STAT4-PD-L1 signaling activation associated with tumor-associated, macrophages-mediated immunosuppression in primary glioblastomas. J ImmunoTher Cancer. 2021;9:e002451.
65. Zhang Y, Yang QF, Zeng XY, Wang MX, Dong S, Yang B, et al. MET amplification attenuates lung tumor response to immunotherapy by inhibiting STING. Cancer Discov. 2021;11:2726–37.
66. Doppelt-Flikshtain O, Asbi T, Younis A, Ginesin O, Cohen Z, Tamari T, et al. Inhibition of osteosarcoma metastasis *in vivo* by targeted downregulation of MMP1 and MMP9. Matrix Biol. 2024;134:48–58.
67. Mummidi S, Das NA, Carpenter AJ, Yoshida T, Yariswamy M, Mostany R, et al. RECK suppresses interleukin-17/TRAF3IP2-mediated MMP-13 activation and human aortic smooth muscle cell migration and proliferation. J Cell Physiol. 2019;234:22242–59.
68. Wolf M, Maltseva I, Clay SM, Pan P, Gajjala A, Chan MF. Effects of MMP12 on cell motility and inflammation during corneal epithelial repair. Exp Eye Res. 2017;160:11–20.
69. McDonald JA. Canonical and noncanonical roles of Par-1/MARK kinases in cell migration. Int Rev Cell Mol Biol. 2014;312:169–99.
70. Marshall EA, Ng KW, Anderson C, Hubaux R, Thu KL, Lam WL, et al. Gene expression analysis of microtubule affinity-regulating kinase 2 in non-small cell lung cancer. Genom Data. 2015;6:145–8.
71. Tahira Y, Sakai K, Sato H, Imamura R, Matsumoto K. Dimer interface in natural variant NK1 is dispensable for HGF-dependent MET receptor activation. Int J Mol Sci. 2021;22:9240.
72. Cheng G, Sun X, Wang J, Xiao G, Wang X, Fan X, et al. HIC1 silencing in triple-negative breast cancer drives progression through misregulation of LCN2. Cancer Res. 2014;74:862–72.
73. Cerdido S, Abrisqueta M, Sanchez-Beltran J, Lambertos A, Castejon-Grinan M, Munoz C, et al. MGRN1 depletion promotes intercellular adhesion in melanoma by upregulation of E-cadherin and inhibition of CDC42. Cancer Lett. 2024;581: 216484.
74. Li Z, Li T, Yates ME, Wu Y, Ferber A, Chen L, et al. The estrogene database reveals diverse temporal, context-dependent, and bidirectional estrogen receptor regulomes in breast cancer. Cancer Res. 2023;83:2656–74.
75. Redmer T, Raigel M, Sternberg C, Ziegler R, Probst C, Lindner D, et al. JUN mediates the senescence associated secretory phenotype and immune cell recruitment to prevent prostate cancer progression. Mol Cancer. 2024;23:114.
76. Lai CB, Mager DL. Role of runt-related transcription factor 3 (RUNX3) in transcription regulation of natural cytotoxicity receptor 1 (NCR1/NKp46), an activating natural killer (NK) cell receptor. J Biol Chem. 2012;287:7324–34.
77. Riccardo F, Barutello G, Petito A, Tarone L, Conti L, Arigoni M, et al. Immunization against ROS1 by DNA electroporation impairs K-Ras-driven lung adenocarcinomas. Vaccines (Basel). 2020;8:166.
78. Jahid S, Sun J, Gelincik O, Blecua P, Edelmann W, Kucherlapati R, et al. Inhibition of colorectal cancer genomic copy number alterations and chromosomal fragile site tumor suppressor FHIT and WWOX deletions by DNA mismatch repair. Oncotarget. 2017;8:71574–86.
79. Jiang X, Wang J, Deng X, Xiong F, Ge J, Xiang B, et al. Role of the tumor microenvironment in PD-L1/PD-1-mediated tumor immune escape. Mol Cancer. 2019;18:10.
80. Jin HT, Ahmed R, Okazaki T. Role of PD-1 in regulating T-cell immunity. Curr Top Microbiol Immunol. 2011;350:17–37.
81. Salmaninejad A, Valilou SF, Shabgah AG, Aslani S, Alimardani M, Pasdar A, et al. PD-1/PD-L1 pathway: Basic biology and role in cancer immunotherapy. J Cell Physiol. 2019;234:16824–37.

82. Li KT, Yuan Z, Lyu JT, Ahn E, Davis SJ, Ahmed R, et al. PD-1 suppresses TCR-CD8 cooperativity during T-cell antigen recognition. Nat Commun. 2021;12:2746.
83. Patsoukis N, Duke-Cohan JS, Chaudhri A, Aksoylar HI, Wang Q, Council A, et al. Interaction of SHP-2 SH2 domains with PD-1 ITSM induces PD-1 dimerization and SHP-2 activation. Commun Biol. 2020;3:128.
84. Alsaab HO, Sau S, Alzhrani R, Tatiparti K, Bhise K, Kashaw SK, et al. PD-1 and PD-L1 checkpoint signaling inhibition for cancer immunotherapy: Mechanism, combinations, and clinical outcome. Front Pharmacol. 2017;8:561.
85. Cao Y, Zhang L, Kamimura Y, Ritprajak P, Hashiguchi M, Hirose S, et al. B7–H1 overexpression regulates epithelial-mesenchymal transition and accelerates carcinogenesis in skin. Cancer Res. 2011;71:1235–43.
86. Zou W, Wolchok JD, Chen L. PD-L1 (B7–H1) and PD-1 pathway blockade for cancer therapy: Mechanisms, response biomarkers, and combinations. Sci Transl Med. 2016;8:328rv4.
87. Yuan Y, Adam A, Zhao C, Chen H. Recent advancements in the mechanisms underlying resistance to PD-1/PD-L1 blockade immunotherapy. Cancers (Basel). 2021;13:663.
88. Ferrara N, Gerber HP, LeCouter J. The biology of VEGF and its receptors. Nat Med. 2003;9:669–76.
89. Chatterjee S, Heukamp LC, Siobal M, Schöttle J, Wieczorek C, Peifer M, et al. Tumor VEGF:VEGFR2 autocrine feed-forward loop triggers angiogenesis in lung cancer. J Clin Invest. 2013;123:1732–40.
90. Shang P, Gao R, Zhu Y, Zhang X, Wang Y, Guo M, et al. VEGFR2-targeted antibody fused with IFN α mut regulates the tumor microenvironment of colorectal cancer and exhibits potent anti-tumor and anti-metastasis activity. Acta Pharm Sin B. 2021;11:420–33.
91. Chen J, Jiang CC, Jin L, Zhang XD. Regulation of PD-L1: a novel role of pro-survival signalling in cancer. Ann Oncol. 2016;27:409–16.
92. Pinato DJ, Black JR, Trousil S, Dina RE, Trivedi P, Mauri FA, et al. Programmed cell death ligands expression in phaeochromocytomas and paragangliomas: Relationship with the hypoxic response, immune evasion and malignant behavior. Oncoimmunology. 2017;6: e1358332.
93. Kythreotou A, Siddique A, Mauri FA, Bower M, Pinato DJ. PD-L1. J Clin Pathol. 2018;71:189–94.
94. Danhier F. To exploit the tumor microenvironment: Since the EPR effect fails in the clinic, what is the future of nanomedicine? J Control Release. 2016;244:108–21.
95. Menna P, Minotti G, Salvatorelli E. Cardiotoxicity of targeted cancer drugs: concerns, "The cart before the horse," and lessons from trastuzumab. Curr Cardiol Rep. 2019;21:33.
96. Bakhtiar R. Antibody drug conjugates. Biotechnol Lett. 2016;38:1655–64.
97. Abdel-Rahman O. Association between PD-L1 inhibitor, tumor site and adverse events of potential immune etiology within the US FDA adverse event reporting system. Immunotherapy-Uk. 2021;13:1407–17.
98. Fan ZW, Wu CY, Chen MM, Jiang YY, Wu YY, Mao RF, et al. The generation of PD-L1 and PD-L2 in cancer cells: From nuclear chromatin reorganization to extracellular presentation. Acta Pharm Sin B. 2022;12:1041–53.
99. Hou W, Yuan Q, Yuan X, Wang Y, Mo W, Wang H, et al. A novel tetravalent bispecific antibody targeting programmed death 1 and tyrosine-protein kinase Met for treatment of gastric cancer. Invest New Drugs. 2019;37:876–89.
100. Harwood SL, Alvarez-Cienfuegos A, Nuñez-Prado N, Compte M, Hernández-Pérez S, Merino N, et al. ATTACK, a novel bispecific T cell-recruiting antibody with trivalent EGFR binding and monovalent CD3 binding for cancer immunotherapy. Oncoimmunology. 2017;7: e1377874.
101. Zhao JL, Wu Y, Xiao T, Cheng C, Zhang T, Gao ZY, et al. A specific anti-cyclin D1 intrabody represses breast cancer cell proliferation by interrupting the cyclin D1-CDK4 interaction. Breast Cancer Res Tr. 2023;198:555–68.
102. Pastushok L, Fu YP, Lin L, Luo Y, DeCoteau JF, Lee K, et al. A Novel Cell-Penetrating Antibody Fragment Inhibits the DNA Repair Protein RAD51. Sci Rep-Uk. 2019;9:11227.
103. Abdeldaim DT, Schindowski K. Fc-Engineered Therapeutic Antibodies: Recent Advances and Future Directions. Pharmaceutics. 2023;15:2402.
104. Xu MY, Bi JH, Liang B, Wang XY, Mo R, Feng N, et al. PEGylation Prolongs the Half-Life of Equine Anti-SARS-CoV-2 Specific $F(ab')_2$. Int J of Mol Sci. 2023;24:3387.
105. Zhou FY, Kroetsch A, Nguyen VP, Huang X, Ogoke O, Parashurama N, et al. High-Affinity Antibody Detection with a Bivalent Circularized Peptide Containing Antibody-Binding Domains. Biotechnol J. 2019;14:e1800647.
106. Alradwan I, Zhi P, Zhang T, Lip H, Zetrini A, He CS, et al. Nanoparticulate drug combination inhibits DNA damage repair and PD-L1 expression in BRCA-mutant and wild type triple-negative breast cancer. J Control Release. 2025;377:661–74.
107. Akbarzadeh F, Khoshgard K. Enhancement of the effect of novel targeted 5-aminolevulinic acid conjugated bismuth oxide nanoparticles-based photodynamic therapy by simultaneous radiotherapy on KB cells. Photodiagn Photodyn. 2024;46:104025.
108. Wang X, Jing ZQ, Huang XB, Liu XY, Zhang YJ, Wang ZJ, et al. PD-L1 antibody conjugated dihydrotanshinone I-loaded polymeric nanoparticle for targeted cancer immunotherapy combining PD-L1 blockade with immunogenic cell death. Int J Pharmaceut. 2024;667(Pt B):125004.
109. Schmidt A, Oberle N, Weiss EM, Vobis D, Frischbutter S, Baumgrass R, et al. Human regulatory T Cells rapidly suppress T Cell receptor-induced Ca^{2+}, NF-κB, and NFAT signaling in conventional T Cells. Sci Signaling. 2011;4:ra90.
110. Tu Y, Liu L, Zhao D, Liu Y, Ma X, Fan Y, et al. Overexpression of miRNA-497 inhibits tumor angiogenesis by targeting VEGFR2. Sci Rep. 2015;5:13827.
111. Lu B, Liu GL, Yu F, Li WJ, Xiang XX, Xiao HZ. MicroRNA-16/VEGFR2/p38/NF-κB signaling pathway regulates cell growth of human pituitary neoplasms. Oncol Rep. 2018;39:1235–44.
112. Dvinge H, Git A, Gräf S, Salmon-Divon M, Curtis C, Sottoriva A, et al. The shaping and functional consequences of the microRNA landscape in breast cancer. Nature. 2013;497:378–82.
113. Zhang L, Li YD, Wang QC, Chen Z, Li XY, Wu ZX, et al. The PI3K subunits, P110α and P110β are potential targets for overcoming P-gp and BCRP-mediated MDR in cancer. Mol Cancer. 2020;19:10.
114. Zhang CF, Wang K, Tao JH, Zheng CJ, Zhai LZ. MYC-dependent MiR-7-5p regulated apoptosis and autophagy in diffuse large B cell lymphoma by targeting AMBRA1. Mol Cell Biochem. 2025;480:191–202.
115. Zhao S, Liu Y, Wang J, Wen Y, Wu BT, Yang DJ, et al. ADSCs increase the autophagy of chondrocytes through decreasing miR-7–5p in Osteoarthritis rats by targeting ATG4A. Int Immunopharmacol. 2023;120:110390.
116. Sletten M, Skogstrom KB, Lind SM, Tinholt M, Stavik B, Rayner S, et al. Elevated TFPI is a prognostic factor in hepatocellular carcinoma: Putative role of miR-7–5p and miR-1236–3p. Thromb Res. 2024;241:109073.
117. Mohan N, Luo X, Shen Y, Olson Z, Agrawal A, Endo Y, et al. A novel bispecific antibody targeting EGFR and VEGFR2 is effective against triple negative breast cancer via multiple mechanisms of action. Cancers. 2021;13:1027.
118. Barzaman K, Samadi M, Moradi-Kalbolandi S, Majidzadeh AK, Salehi M, Jalili N, et al. Development of a recombinant anti-VEGFR2-EPCAM bispecific antibody to improve antiangiogenic efficiency. Exp Cell Res. 2021;405:112685.
119. Lin RK, Zhang L, Ye BW, Wang YA, Li YD, Jason H, et al. A multi-functional nano-system combining PI3K-110α/β inhibitor overcomes P-glycoprotein mediated MDR and improves anti-cancer efficiency. Cancer Lett. 2023;563:216181.
120. Kim SY, Yasuda S, Tanaka H, Yamagata K, Kim H. Non-clustered protocadherin Cell Adh Migr. 2011;5:97–105.
121. Dallosso AR, Øster B, Greenhough A, Thorsen K, Curry TJ, Owen C, et al. Long-range epigenetic silencing of chromosome 5q31 protocadherins is involved in early and late stages of colorectal tumorigenesis through modulation of oncogenic pathways. Oncogene. 2012;31:4409–19.
122. Asad M, Wong MK, Tan TZ, Choolani M, Low J, Mori S, et al. FZD7 drives in vitro aggressiveness in Stem-A subtype of ovarian cancer via regulation of non-canonical Wnt/PCP pathway. Cell Death Dis. 2014;5: e1346.
123. Wang Y. Wnt/Planar cell polarity signaling: a new paradigm for cancer therapy. Mol Cancer Ther. 2009;8:2103–9.
124. Faura Tellez G, Vandepoele K, Brouwer U, Koning H, Elderman RM, Hackett TL, et al. Protocadherin-1 binds to SMAD3 and suppresses TGF-β1-induced gene transcription. Am J Physiol Lung Cell Mol Physiol. 2015;309:L725-35.
125. Vega-Benedetti AF, Loi E, Moi L, Blois S, Fadda A, Antonelli M, et al. Clustered protocadherins methylation alterations in cancer. Clin Epigenetics. 2019;11:100.
126. Jin L, Zhu C, Wang X, Li C, Cao C, Yuan J, et al. Urocortin attenuates TGFβ1-induced Snail1 and slug expressions: inhibitory role of Smad7 in Smad2/3 signaling in breast cancer cells. J Cell Biochem. 2015;116:2494–503.

127. Wang J, Xu Y, Xu Y, Zhu H, Zhang R, Zhang G, et al. Urocortin's inhibition of tumor growth and angiogenesis in hepatocellular carcinoma via corticotrophin-releasing factor receptor 2. Cancer Invest. 2008;26:359–68.
128. Florio P, De Falco G, Leucci E, Torricelli M, Torres PB, Toti P, et al. Urocortin expression is downregulated in human endometrial carcinoma. J Endocrinol. 2006;190:99–105.
129. Owens GL, Lawrence KM, Jackson TR, Crosbie EJ, Sayan BS, Kitchener HC, et al. Urocortin suppresses endometrial cancer cell migration via CRFR2 and its system components are differentially modulated by estrogen. Cancer Med. 2017;6:408–15.
130. Han SW, Jung YK, Lee EJ, Park HR, Kim GW, Jeong JH, et al. DICAM inhibits angiogenesis via suppression of AKT and p38 MAP kinase signalling. Cardiovasc Res. 2013;98:73–82.
131. Jung YK, Han SW, Kim GW, Jeong JH, Kim HJ, Choi JY. DICAM inhibits osteoclast differentiation through attenuation of the integrin αVβ3 pathway. J Bone Miner Res. 2012;27:2024–34.
132. Dong ZQ, Guo ZY, Xie J. The lncRNA EGFR-AS1 is linked to migration, invasion and apoptosis in glioma cells by targeting miR-133b/RACK1. Biomed Pharmacother. 2019;118: 109292.
133. Yuan S, Luan X, Chen H, Shi X, Zhang X. Long non-coding RNA EGFR-AS1 sponges micorRNA-381 to upregulate ROCK2 in bladder cancer. Oncol Lett. 2020;19:1899–905.
134. Qi H, Wang S, Wu J, Yang S, Gray S, Ng CSH, et al. EGFR-AS1/HIF2A regulates the expression of FOXP3 to impact the cancer stemness of smoking-related non-small cell lung cancer. Ther Adv Med Oncol. 2019;11:1758835919855228.
135. Lin CC, Yang WH, Lin YT, Tang X, Chen PH, Ding CC, et al. DDR2 upregulation confers ferroptosis susceptibility of recurrent breast tumors through the Hippo pathway. Oncogene. 2021;40:2018–34.
136. Velmurugan BK, Chang WH, Chung CM, Yeh CM, Lee CH, Yeh KT, et al. DDR2 overexpression in oral squamous cell carcinoma is associated to lymph node metastasis. Cancer Biomark. 2018;22:747–53.
137. Zhang K, Corsa CA, Ponik SM, Prior JL, Piwnica-Worms D, Eliceiri KW, et al. The collagen receptor discoidin domain receptor 2 stabilizes SNAIL1 to facilitate breast cancer metastasis. Nat Cell Biol. 2013;15:677–87.
138. Liu QQ, Liu YW, Xie YK, Zhang JH, Song CX, Wang JZ, et al. Amplification of DDR2 mediates sorafenib resistance through NF-κB/c-Rel signaling in hepatocellular carcinoma. Cell Biol Int. 2021;45:1906–16.
139. Xie B, Lin W, Ye J, Wang X, Zhang B, Xiong S, et al. DDR2 facilitates hepatocellular carcinoma invasion and metastasis via activating ERK signaling and stabilizing SNAIL1. J Exp Clin Cancer Res. 2015;34:101.
140. Wang YG, Xu L, Jia RR, Wu Q, Wang T, Wei J, et al. DDR2 induces gastric cancer cell activities via activating mTORC2 signaling and is associated with clinicopathological characteristics of gastric cancer. Dig Dis Sci. 2016;61:2272–83.
141. Tu MM, Lee FYF, Jones RT, Kimball AK, Saravia E, Graziano RF, et al. Targeting DDR2 enhances tumor response to anti-PD-1 immunotherapy. Sci Adv. 2019;5:eaav2437.
142. Gibbs GM, Roelants K, O'Bryan MK. The CAP superfamily: cysteine-rich secretory proteins, antigen 5, and pathogenesis-related 1 proteins–roles in reproduction, cancer, and immune defense. Endocr Rev. 2008;29:865–97.
143. Hazell GG, Peachey AM, Teasdale JE, Sala-Newby GB, Angelini GD, Newby AC, et al. PI16 is a shear stress and inflammation-regulated inhibitor of MMP2. Sci Rep. 2016;6:39553.
144. van Hinsbergh VW, Koolwijk P. Endothelial sprouting and angiogenesis: matrix metalloproteinases in the lead. Cardiovasc Res. 2008;78:203–12.

Publisher's Note